TEL AVIV UNIVERSITY
RAYMOND AND BEVERLY SACKLER
FACULTY OF EXACT SCIENCES

Pomeron structure and diffractive parton distributions

Thesis submitted toward the M.Sc. Degree
at Tel Aviv University
School of Physics and Astronomy

by
Michael Groys

July 3, 2005

The research work for this thesis was carried out in the Experimental High Energy Physics Group of the Tel Aviv University under the supervision of Prof. Halina Abramowicz and Prof. Aharon Levy.

Abstract

Measurements of the diffractive structure function, F_2^D, of the proton at HERA are used to extract the partonic structure of the Pomeron. Regge Factorization is tested and is found to describe well the existing data within the selected kinematic range. The analysis is based on the next to leading order QCD evolution equations. The results obtained from various data sets are compared. An analysis of the uncertainties in determining the parton distributions is provided. The probability of diffraction is calculated using the obtained results.

Contents

1 Introduction **4**

2 Theoretical Framework **7**
2.1 Deep Inelastic Scattering 7
2.2 Diffraction and the Pomeron 8
2.3 DIS Formalism 10
2.4 Diffractive DIS formalism 11
2.5 Diffractive parton distributions 13
2.6 Regge Theory 14
2.7 Regge factorization 16
2.8 Pomeron structure functions and PDFs 17

3 Experimental Data **18**
3.1 Signatures of Diffraction 18
3.2 Proton Dissociation 19
3.3 HERA data 20

4 Data Selection **22**
4.1 Cut on $x_{I\!P}$ 22
4.2 Cut on Q^2 23
4.3 Cut on M_X 23

5 Regge Factorization test **24**
5.1 Test of Q^2 independence 24
5.2 Test of β dependence 28
5.3 Conclusion of the factorization test 28

6 Computations **31**
6.1 Comparison of QCDNUM and CTEQ packages 31
6.2 Fitting proceedure 34
6.3 Outline of the calculations 35

7 Fits **36**
7.1 Fit Results 36
7.2 Fit presentation 36
7.3 Comparison of the different fits 44

8 Results interpretation **46**
8.1 Momentum carried by quarks and gluons 46
8.2 Probability of diffraction 48

9 Summary and Conclusions **51**

Bibliography **53**

Appendix: Experimental data references **56**

1 Introduction

A large fraction (about 10%) of deep inelastic scattering (DIS) events in *ep* interactions at the HERA collider, have all the characteristics typical of *diffractive* scattering (see Fig. 1). In these events the proton remains intact and loses very little momentum. One of the most important experimental characteristic of diffractive events at high energy is a large rapidity gap between the proton and the system X.

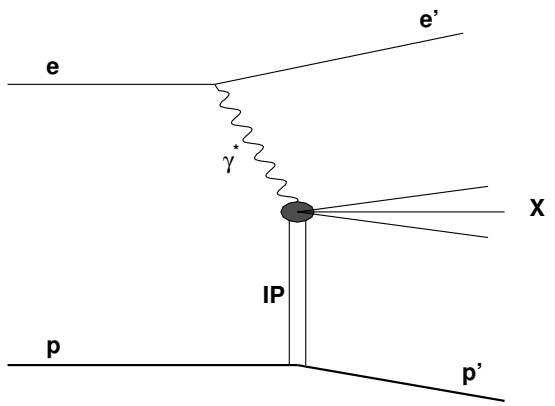

Figure 1: *Diagram of a diffractive single dissociation event at HERA.*

Theoretically, diffraction can be described by the exchange of a colorless object with vacuum quantum numbers between the interacting particles, the virtual photon and the proton in case of DIS. In *soft* interactions, where a small fraction of energy is exchanged, this colorless object is identified as the Pomeron.

The notion of the Pomeron comes from Regge theory of strong interactions [1]. The Pomeron was first introduced by Gribov [2] and represents a universal trajectory with the quantum numbers of the vacuum. In the language of Quantum Chromodynamics, the candidate for vacuum exchange with properties similar to the soft Pomeron is two gluon exchange [6]. As a result of interactions between the two gluons, a ladder structure develops. However in perturbative QCD, the properties of this ladder depend on the energy and scales involved in the interactions, implying its non universal character.

There is no strict theory for diffractive scattering. Within the Ingelman and Schlein model[5], diffractive processes are assumed to proceed in two steps. First the Pomeron is emitted from the proton. In the second step it interacts with a probe particle. As with ordinary DIS, a QCD factorization theorem has been proven to hold [7] also for diffractive processes initiated by a lepton beam. This view allows to use Regge theory to describe Pomeron propagation and to use QCD factorization in order to describe the interaction between the Pomeron and the probe particle. The obtained parton distribution functions satisfy the usual DGLAP [17, 18, 19] evolution equations.

Ingelman and Schlein [5] were the first to propose to probe the Pomeron structure in hard scattering processes. In their paper they investigated proton-antiproton interactions at the CERN SPS collider. They also mentioned the experimental signature of diffraction - the existence of large rapidity gap.

It is not simple to define what is meant by a diffractive event. One has to be sure that the event was produced in a process where vacuum quantum numbers were exchanged. In high energy interactions, the clearest definition of a diffractive process is one where a large rapidity gap was produced which is not exponentially suppressed [20]. However, this definition is not always practical for the experimental selection of diffractive events.

In the last 10 years a large amount of diffractive data was accumulated at the HERA collider [8, 9, 10]. There are three methods used at HERA to select diffractive events. One [10] uses the Leading Proton Spectrometer (LPS) to detect the scattered proton and by choosing the kinematic region where the scattered proton looses very little of its initial longitudinal energy, it ensures that the event was diffractive. A second method [9] simply request a large rapidity gap (LRG) in the event and fits the data to contributions coming from Pomeron and Reggeon exchange. The third method [8] uses the distribution of the mass of the hadronic system seen in the detector, M_X, to isolate diffractive events. We will refer to these three as ZEUS LPS, H1 and ZUES FPC[1] methods. We will discuss in the data selection section the implications of these three different methods on the results.

The experiments [11, 12, 13] provide sets of results for inclusive diffractive structure function, $x_{I\!P} F_2^{D(3)}$, in different regions of phase space. The general approach in analyzing these diffractive data is to parameterize theoretical model with some set of free parameters. Then the best values of these parameters can be obtained by fitting the model to the experimental data. In previous works, different data sets were analyzed and fits to them were provided. However no systematic comparison of different data sets was

[1] A Forward Plug Calorimeter (FPC) is used in this analysis

done. Moreover, the longitudinal structure function was always neglected. Most fits were based on the Regge factorization assumption (§2.7) with different parameterizations of the initial Pomeron parton distribution functions (PDF).

In the present study, Regge factorization is tested. New fits are provided and include the contribution of the longitudinal structure function. The obtained PDFs are systematically analyzed. A comparison of the different experimental data sets is provided. Additional quantities derived from the fit results are also presented.

2 Theoretical Framework

2.1 Deep Inelastic Scattering

General DIS events are of the following form:

$$l(k) + p(P) \rightarrow l(k') + X. \tag{1}$$

At the HERA collider ep scattering is studied. The dominant processes at relatively small momentum transfer at the lepton vertex ($Q^2 \ll M_Z^2$) are those where a virtual photon (γ^*) is exchanged (see fig. 2).

The kinematic variables which are commonly used in the description of DIS

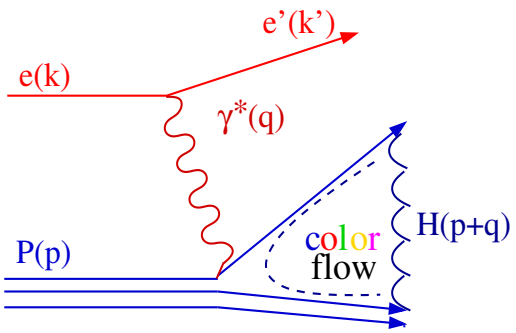

Figure 2: *The dominant DIS process at the HERA collider. The exchanged particle is a virtual photon (γ^*). $H(p+q)$ represents outgoing hadrons of total four-momentum $p+q$.*

events are,

$$Q^2 \equiv -(k-k')^2\,, \tag{2}$$

$$W^2 \equiv (p+q)^2\,, \tag{3}$$

$$s \equiv (p+k)^2\,, \tag{4}$$

$$x \equiv \frac{Q^2}{2p\cdot q}\,, \tag{5}$$

$$y \equiv \frac{p\cdot q}{p\cdot k} = \frac{Q^2}{sx}\,. \tag{6}$$

Where

- Q^2 is the negative four momentum transfer squared from the electron,
- W is the center of mass energy of the virtual photon-proton system,
- s is the center of mass energy squared of the electron-proton system,
- x can be interpreted as the fraction of the proton four momentum carried by the struck quark and
- y, which in the proton rest frame is the fraction of the electron energy transferred to the proton.

2.2 Diffraction and the Pomeron

The *diffractive* events are a subset of DIS events. These events are characterized by an outgoing proton that carries a large fraction (> 0.9) of the initial proton momentum. The other products of the reaction are separated from the proton by a large rapidity gap (LRG), see §3.1.

The diffractive processes studied at HERA are of the form (see fig. 1):

$$e(k) + p(p) \rightarrow e(k') + p'(p^{'}) + X. \tag{7}$$

This type of processes is also called *single diffractive dissociation*. A diagram for diffractive scattering is presented in Fig. 3.

According to the Ingelman and Schlein model [5] the diffractive process (7) can be decomposed into two parts. The first part is an emission of some object by the proton and the second one is the deep inelastic scattering of virtual photon, emitted by the electron, off such an object.

Then the interaction of virtual photon with the proton can be written as,

$$\gamma^* + p \quad \xrightarrow{I\!P} \quad X + p. \tag{8}$$

If the momentum fraction carried by the exchanged object is less than 1% of the proton momentum (in the infinite momentum frame) we consider this to be largely due to *Pomeron* exchange. The Pomeron has vacuum quantum numbers (in particular it must be colorless).

The interaction between an energetic virtual photon and the Pomeron can be described by perturbative QCD. On the other hand the kinematic behavior of the Pomeron and the proton-Pomeron coupling lies in the non-perturbative region. It is assumed to be described by *Regge Theory* (§2.6). In order to use Regge theory with perturbative QCD - *Regge factorization* (§2.7) is assumed.

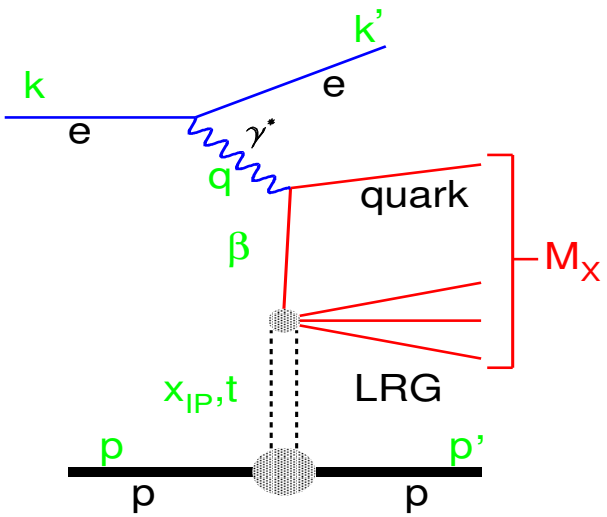

Figure 3: *Schematic diagram for diffractive DIS in ep interactions.*

QCD factorization theorem allows us to represent diffractive cross section in terms of diffractive parton distribution functions (See §2.5). Combining this with Regge factorization allows us to introduce Pomeron parton distribution functions (§2.8). Then we can use the regular QCD DIS formalism (§2.3) in order to evaluate the $\gamma^* I\!P$ vertex.

The X system, from processes (8), has a limited mass compared to the overall available energy. It may consist of a set of hadrons in which case it is called inclusive diffraction, but it may also consist of a single hadron. In the latter case the hadron must carry the quantum numbers of the photon as do the vector mesons. The corresponding process is called *exclusive vector meson electro-production*.

In the current work we will study the structure and properties of the Pomeron by analyzing inclusive diffraction data from the HERA collider.

Three additional variables are used to describe diffractive processes. The t variable represents the change in the proton four momentum squared as a result of the interaction,

$$t \equiv (p - p^{'})^2 \,. \tag{9}$$

In this study we are working in the Breit (infinite momentum) frame. There are two variables that describe the Pomeron in this approach. The first is $x_{I\!P}$ (Eq. (10)) which is equal to the fraction of the proton momentum carried by the Pomeron. The second one is β (Eq. (11)) which represents the fraction of the Pomeron momentum carried by the struck quark. This variable is

equivalent to the Bjorken variable x but relative to the target Pomeron.

$$x_{I\!P} = \frac{q(p-p')}{q\cdot p} = \frac{M_X^2+Q^2-t}{W^2+Q^2-m_P^2} \approx \frac{M_X^2+Q^2}{W^2+Q^2}, \tag{10}$$

$$\beta = \frac{Q^2}{2q\cdot(p-p')} = \frac{Q^2}{M_X^2+Q^2-t} \approx \frac{Q^2}{M_X^2+Q^2}. \tag{11}$$

The following relation holds:

$$x = x_{I\!P}\beta. \tag{12}$$

The physical meaning of the variables is shown in fig. 3.

2.3 DIS Formalism

In this section the general formalism of DIS will be discussed. Consider ep deep inelastic scattering in a region where γ^* exchange dominates. Its cross section can be expressed using the usual dimensionless variables in the following way:

$$\frac{d^2\sigma}{dx\ dy} = \frac{4\pi\alpha^2 s}{Q^4}\left(\frac{y^2}{2}2xF_1(x,Q^2)+(1-y)F_2(x,Q^2)\right). \tag{13}$$

The structure functions F_1 and F_2 are process dependent. In the quark parton model (QPM) the nucleon is believed to consist of almost free partons (quarks and gluons). QCD factorization theorem states that the cross section for lepton nucleon at large Q^2 can be represented as an incoherent sum of lepton quark interactions,

$$\frac{d^2\sigma^{ep}}{dx\ dy} = \sum_q \frac{d^2\sigma^{eq}}{dx\ dy}, \tag{14}$$

where q denotes all quark flavors in the proton. In the leading order of perturbative QCD, the structure functions can be expressed as,

$$F_1(x) = \frac{1}{2}\sum_i q_i^2 f_i(x), \tag{15}$$

$$F_2(x) = \sum_i x q_i^2 f_i(x)\,, \tag{16}$$

where q_i stands for the charge of the i-th quark, expressed in units of the electron charge. Then the Callan-Gross relation should hold,

$$2xF_1 = F_2. \tag{17}$$

In QCD, partons interact through the exchange of gluons and so the parton distribution functions become Q^2 dependent. To incorporate these interactions correctly to order α_S in the perturbation expansion the following processes must be considered,

i. gluon bremsstrahlung diagrams,

ii. quark pair production by gluon,

iii. ggg coupling.

The so called *DGLAP evolution equations [17, 18, 19]* provide the mechanism of incorporating such processes into the DIS picture. These equations describe the evolution of parton density functions with Q^2,

$$\frac{dq_i(x,Q^2)}{d\log Q^2} = \frac{\alpha_S}{2\pi}\int_x^1 \frac{dy}{y}\left[q_i(y,Q^2)P_{qq}\left(\frac{x}{y}\right) + g(y,Q^2)P_{qg}\left(\frac{x}{y}\right)\right],, \quad (18)$$

$$\frac{dg_i(x,Q^2)}{d\log Q^2} = \frac{\alpha_S}{2\pi}\int_x^1 \frac{dy}{y}\left[\sum_i q_i(y,Q^2)P_{gq}\left(\frac{x}{y}\right) + g(y,Q^2)P_{gg}\left(\frac{x}{y}\right)\right] . \quad (19)$$

In addition, the emission of non collinear gluons by quarks will induce an appearance of a non-vanishing longitudinal cross section - σ_L. This leads to a violation of the Callan-Gross relation, which can be quantified by the longitudinal structure function defined as

$$F_L = F_2 - 2xF_1. \quad (20)$$

2.4 Diffractive DIS formalism

In an analog to Eq. (13), the diffractive cross section can be written as

$$\frac{d^2\sigma^D}{dx\,dy} = \frac{4\pi\alpha^2 s}{Q^4}\left(\frac{y^2}{2}2xF_1^D(x,Q^2) + (1-y)F_2^D(x,Q^2)\right). \quad (21)$$

To describe general diffractive DIS events we need two more variables, $x_{I\!P}$ and t, in addition to the usual x and Q^2 in the cross section formula. Then using eqs. (20) and (21), the four-fold differential cross section for ep scattering can be written as

$$\frac{d^4\sigma^D}{dx_{I\!P}\,dt\,dx\,dQ^2} = \frac{4\pi\alpha^2}{xQ^2}\left(\left[1-y+\frac{y^2}{2}\right]F_2^{D(4)}(x,Q^2,x_{I\!P},t) - \frac{y^2}{2}F_L^{D(4)}(x,Q^2,x_{I\!P},t)\right). \quad (22)$$

The relation $x = x_{I\!P}\beta$ allows to use any pair of x, $x_{I\!P}$ or β with Q^2 and t in order to uniquely describe diffractive events. It is commonly accepted to use the basis of $x_{I\!P}$ and β. In the latter case, the differential cross section will look like

$$\frac{d^4\sigma^D}{dx_{I\!P}\,dt\,d\beta\,dQ^2} = \frac{4\pi\alpha^2}{\beta Q^2}\left(\left[1-y+\frac{y^2}{2}\right]F_2^{D(4)}(\beta,Q^2,x_{I\!P},t) - \frac{y^2}{2}F_L^{D(4)}(\beta,Q^2,x_{I\!P},t)\right). \tag{23}$$

Let us introduce also the *reduced* cross section, σ_r^D,

$$\frac{d^4\sigma^D}{dx_{I\!P}\,dt\,d\beta\,dQ^2} = \frac{4\pi\alpha^2}{\beta Q^4}\left(1-y+\frac{y^2}{2}\right)\sigma_r^{D(4)}(x_{I\!P},\,t\,,\beta,\,Q^2). \tag{24}$$

From Eq. (24) it follows that,

$$\sigma_r^{D(4)} = F_2^{D(4)} - \frac{y^2}{2(1-y+y^2/2)}F_L^{D(4)}. \tag{25}$$

Two quantitative conclusions can be made,

- $F_L^{D(4)}$ affects $\sigma_r^{D(4)}$ at high y,
- if $F_L^{D(4)} = 0$ then $\sigma_r^{D(4)} = F_2^{D(4)}$.

Most of the time we will work with differential cross sections and structure functions integrated over t,

$$A^{D(3)} = \int dt A^{D(4)}, \tag{26}$$

thus

$$x_{I\!P}\sigma_r^{D(3)} = x_{I\!P}F_2^{D(3)} - \frac{y^2}{2(1-y+y^2/2)}x_{I\!P}F_L^{D(3)}\ . \tag{27}$$

In the experiment, the values of σ_r^D are measured. In order to get the value of F_L^D, the beam energy must be changed. So far it has not be done and thus F_2^D and F_L^D can not be measured independently. Experimentalists often assume that the influence of the longitudinal structure function is negligible. In the current study such an assumption was not made and we consider that the value of $x_{I\!P}F_2^{D(3)}$ as provided by the experimentalists actually corresponds to that of $x_{I\!P}\sigma_r^{D(3)}$ (see Eq. (27)).

2.5 Diffractive parton distributions

J.Collins [23] proved that QCD Factorization theorem holds for diffractive processes. Then the cross section differential in the relevant variables can be written in the form[24],

$$d\sigma = \sum_i \int d\xi \, f_i^{(D)}(\xi, x_{I\!P}, t; \mu) d\hat{\sigma}_i, \tag{28}$$

where,

- the index i is the flavor of the struck parton,
- the variable $\xi \equiv \beta$ is the fractional light-front momentum of the struck parton relative to the Pomeron, and t and $x_{I\!P}$ have their usual definitions,
- the hard-scattering coefficients $d\hat{\sigma}$ are perturbatively calculable and are the same as for the corresponding fully inclusive cross sections,
- the renormalization/factorization scale μ should be of order Q.

The diffractive parton distribution function $f_i^{(D)}$ is to be interpreted as the number density of partons conditional on the observation of a diffractive proton in the final state. This formula obeys the standard DGLAP evolution equation for its μ dependence with the same kernels as for the fully inclusive parton distribution functions (pdfs). For a fixed value of $x_{I\!P}$, the evolution in x and Q^2 is equivalent to the evolution in β and Q^2. The proof of the factorization formula is valid for the direct photoproduction of jets, heavy quarks, etc. However this formula fails for hadron-hadron scattering.

According to Eq. (28), F_2^D can be also decomposed into diffractive parton distributions, f_i^D, in a way similar to the inclusive F_2,

$$\frac{d^2 F_2^D(x, Q^2, x_{I\!P}, t)}{dx_{I\!P}\, dt} = \sum_i \int d\xi \frac{d^2 f_i^D(\xi, x_{I\!P}, t; \mu)}{dx_{I\!P}\, dt} \hat{F}_{2,i}(\xi, Q^2; \mu), \tag{29}$$

where $\hat{F}_{2,i}$ is the universal structure function for DIS on parton i.

An additional quantity that can be defined is the probability of diffraction for the action of the hard probe which couples to a parton i [25],

$$P_i^D(x, Q^2) \;=\; \frac{\int f_i^{(D)}(\beta, Q^2, x_{I\!P}, t)\, \delta(x - x_{I\!P}\beta) dt dx_{I\!P} d\beta}{f_i(x, Q^2)} \tag{30}$$

$$= \frac{\int \frac{1}{x_{I\!P}} f_i^{(D)}\left(\frac{x}{x_{I\!P}}, Q^2, x_{I\!P}, t\right) dt dx_{I\!P}}{f_i(x,Q^2)}$$
$$= \frac{\int \frac{1}{\beta} f_i^{(D)}\left(\beta, Q^2, \frac{x}{\beta}, t\right) dt d\beta}{f_i(x,Q^2)} \; .$$

If the interaction in the gluon sector at small x reaches a strength close to the unitarity limit then P_g is expected to be close to 1/2 and be much larger than P_q.

2.6 Regge Theory

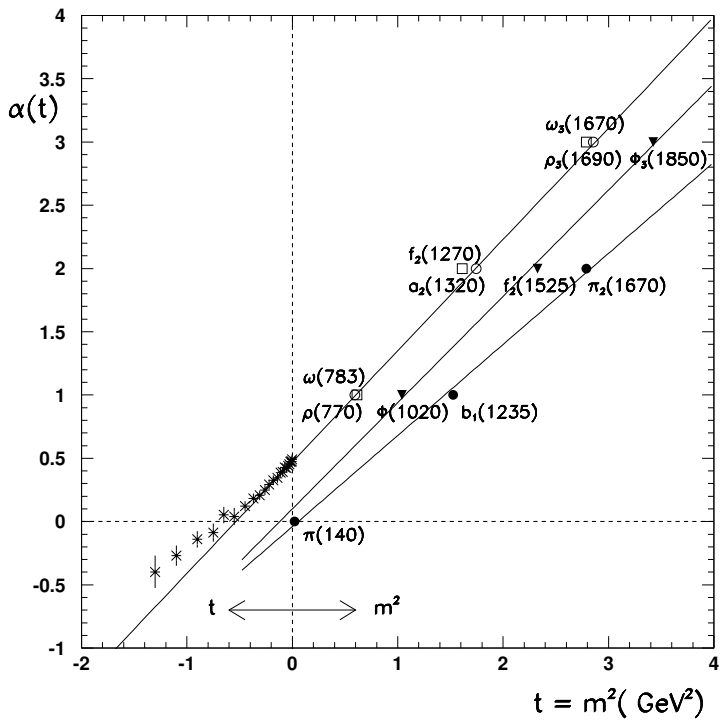

Figure 4: *Example of the ρ (circles), ω (empty squares), ϕ (triangles) and π (dots) trajectories. Also shown is the continuation of the ρ trajectory as measured in $\pi^- p \to \eta n$. (Taken from [22].)*

Experimentally it was found that different particles with the same quantum numbers, but with different spin values, lie on a so-called *Regge trajectory*

$l = \alpha(t)$. This trajectory has the property that for any particle i within the same group – $\alpha(m_i^2) = J_i$, where J_i is the spin of the particle. In fig. 4 trajectories for different set of hadrons are presented. Now it is commonly accepted that all hadrons behave in such way. Moreover most of Regge trajectories can be described as lines in the (J, t) plane and can be parameterized by $\alpha(t) = \alpha_0 + \alpha' t$.

In Quantum field theory, interactions are represented by particle exchange. In QED these particles are photons, for weak interactions there are weak bosons ($W^{\pm}$ and Z), and for QCD this role is played by gluons. To describe strong interactions of hadrons it is useful to consider an exchange not of single particle, but of a whole trajectory. In Regge theory the scattering amplitude is given by

$$A(s,t) \sim s^{\alpha(t)}, \tag{31}$$

where s and t are regular Mandelstam variables (See Eq. (4) and Eq. (9)).

We assume that the *Pomeron* is such a Regge trajectory and it is commonly parameterized as

$$\alpha_{I\!P}(t) = \alpha_{I\!P}(0) + \alpha'_{I\!P} t. \tag{32}$$

From Eq. (31) and Eq. (32) follows that the total hadron-hadron cross section, in the case when the Pomeronis the dominant trajectory, is

$$\sigma_{tot}(ab) \sim s^{\alpha_{I\!P}(0)-1}. \tag{33}$$

Then, using the optical theorem, an expression for the elastic cross section, σ^{el}, can be derived,

$$\frac{d\sigma^{el}}{dt}(ab \to ab) \;=\; \frac{\sigma^2_{tot}(ab)}{16\pi} e^{2(b_0^{el} + \alpha'_{I\!P} \ln s)t}. \tag{34}$$

The expression for the cross section of the diffractive scattering, σ^D, can be obtain by applying Mueller's generalization of the optical theorem [28]. This generalization relates the total cross section of two body scattering with the imaginary part of the forward elastic amplitude, to the case of three body scattering.

$$\frac{d^2\sigma^D}{dt\, dM_X^2}(ab \to Xb) \;\sim\; \frac{1}{M_X^2}\left(\frac{s}{M_X^2}\right)^{2(\alpha_{I\!P}(0)-1)} e^{2\left(b_0^D + \alpha'_{I\!P} \ln \frac{s}{M_x^2}\right)t}. \tag{35}$$

The universality of the Pomeron parameterization (Eq. (32)) has been pointed out by Donnachie and Landshoff. The value of $\alpha_{I\!P}(0) = 1.081$ [14]

and $\alpha'_{I\!P} = 0.25\,\mathrm{GeV}^{-2}$ [15] were derived based on total hadron-proton interaction cross sections and elastic proton-proton data. Recently the $I\!P$ intercept has been reevaluated leading to a value of $\alpha_{I\!P}(0) = 1.096 \pm 0.03$ [21].

In the present analysis the universality of the Pomeron is not assumed and thus $\alpha_{I\!P}$ is treated as a free parameter which best describes the data.

2.7 Regge factorization

Assuming that an interaction is due to the Pomeron exchange we can write

$$F_2^{D(4)} = \frac{N}{16\pi}|\beta_{p\,I\!P}(t)|^2 x_{I\!P}^{1-2\alpha_{I\!P}(t)} F_2^{I\!P}(x_{I\!P},\, t\,,\beta,\, Q^2)\ . \tag{36}$$

Here $\beta_{p\,I\!P}(t)$ represents the Pomeron-proton coupling. It may be obtained from fits to elastic hadron-hadron cross section at small t,

$$\beta_{p\,I\!P}(t) = 4.6 mb^{1/2} e^{1.9 GeV^{-2} t}. \tag{37}$$

$x_{I\!P}^{1-2\alpha_{I\!P}(t)}$ can be treated as the Pomeron propagator.

N is a normalization factor. In general its value is arbitrary as the Pomeron is not a real particle. However if one wishes to impose the momentum sum rule,

$$\sum_i \int_0^1 x q_i(x) dx + \int_0^1 x g(x) dx = 1, \tag{38}$$

then the value of N is important. If one does not care about this rule then the choice of N will result in an overall normalization of Pomeron parton distribution functions. Ingelman and Schlein[5] use $N = 1$, while Donnachie and Landshoff [16] use $N = \frac{2}{\pi}$. We will follow the latter value of this constant without imposing any overall normalization.

Regge factorization states that

$$F_2^{I\!P}(x_{I\!P},\, t\,,\beta,\, Q^2) = F_2^{I\!P}(\beta, Q^2). \tag{39}$$

Thus $F_2^{I\!P}(\beta, Q^2)$ can be treated as the Pomeron structure function. To simplify expressions we will introduce the Pomeron flux factor,

$$f_{I\!P/p}(x_{I\!P},\, t) = \frac{N}{16\pi}\,|\beta_{p\,I\!P}(t)|^2 x_{I\!P}^{1-2\alpha_{I\!P}(t)}. \tag{40}$$

Then diffractive structure functions become,

$$F_2^{D(4)}\,(x_{I\!P},\, t\,,\beta,\, Q^2) = \quad f_{I\!P/p}(x_{I\!P},\, t)\, F_2^{I\!P}\,(\beta,\, Q^2), \tag{41}$$

$$F_1^{D(4)}\,(x_{I\!P},\, t\,,\beta,\, Q^2) = \quad f_{I\!P/p}(x_{I\!P},\, t)\, \tfrac{1}{x_{I\!P}}\, F_1^{I\!P}\,(\beta,\, Q^2), \tag{42}$$

$$F_L^{D(4)}\,(x_{I\!P},\, t\,,\beta,\, Q^2) = \quad f_{I\!P/p}(x_{I\!P},\, t)\, F_L^{I\!P}\,(\beta,\, Q^2). \tag{43}$$

2.8 Pomeron structure functions and PDFs

In the Ingelman-Schlein model it is assumed that the structure functions of the Pomeron are defined in exactly the same way as the structure functions of the proton. This is equivalent to using QCD factorization for diffraction together with the assumption of validity of Regge Factorization. Using this assumption we can write,

$$f^D_{q,g}(x_{I\!P}, Q^2, \beta) = f_{I\!P/P}(x_{I\!P}) f_{q,g/I\!P}(Q^2, \beta). \tag{44}$$

This allows to calculate the Pomeron structure functions in terms of the Pomeron parton distribution functions. In order to obtain the Pomeron pdfs at any Q^2 we can guess it at some initial scale, Q^2_{ini}, and then evolve it using regular DGLAP evolution equations.

It is well established from conventional Regge phenomenology that the Pomeron is self-charge-conjugate and isoscalar. This implies some constraints on the Pomeron pdfs.

- the density of any flavor of anti-quark is equal to the density of the corresponding quark,

$$f_{q/I\!P}(x) = f_{\bar{q}/I\!P}(x), \tag{45}$$

- the densities of the up and down quarks and antiquarks are equal,

$$f_{u/I\!P}(x) = f_{d/I\!P}(x) = f_{\bar{u}/I\!P}(x) = f_{\bar{d}/I\!P}(x) = f_{q/I\!P}(x). \tag{46}$$

In the *massless scheme* it is assumed that,

$$f_q(x, Q^2) = 0 \text{ for } Q^2 < 4m_q^2. \tag{47}$$

Above this threshold, the quark is assumed to be massless.

In that scheme at an initial scale of $Q^2_{ini} = 3\,\mathrm{GeV}^2$ only 3 quarks appear. The heavy quarks (charm and bottom) are generally considered heavy enough so that their densities can be correctly generated dynamically, by evolution from the known light parton and gluon densities.

There are different approaches to define the initial strange quark density. One approach is to set it to 0 at the initial scale [26]. Another possibility is to set $f_{s/I\!P}(x) = f_{u/I\!P}(x)$. In general the strange quark density can be defined as,

$$f_{s/I\!P}(x) = s f_{u/I\!P}(x), \tag{48}$$

where s is a suppression factor ($0 \leq s \leq 1$). Often it is chosen to be $s = 0.3$ [27]. In the current work we will assume that the $s = 0$ [26].

To a good first approximation there are only two parton densities to start with: the gluon density, $f_{g/I\!P}$, and the quark density, $f_{q/I\!P}$.

3 Experimental Data

3.1 Signatures of Diffraction

In general in diffractive processes (7), where the target preserves its identity, the square of the momentum transfer t tends to be limited [4]. At high energy, the kinematics of producing two low mass outgoing states (X and p) with a small fraction of momentum exchanged between them leads to a large rapidity gap (LRG), (see fig. 5 taken from [22]).

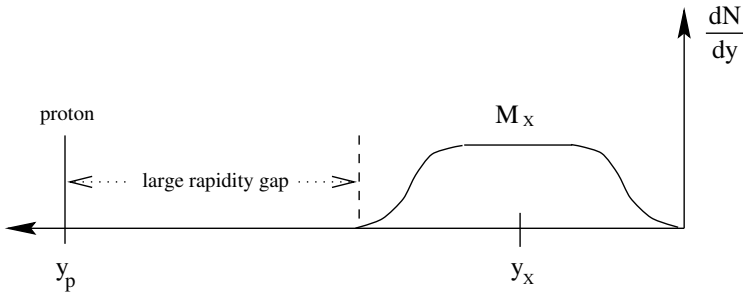

Figure 5: *Schematic representation of rapidity (y) distribution for single diffraction events.*

To estimate LRG lets assume that $t = 0$ (for the real events $|t| < 2\,\mathrm{GeV}^2$, so it is a good assumption). Then in the center of mass system of $\gamma^* p$, the outgoing proton and the system X move in opposite directions, with longitudinal momentum $p_L \approx W/2$. The rapidities of the proton and the system X are respectively:

$$y_P = \tfrac{1}{2} \ln \tfrac{E_P + p_L}{E_P - p_L} \approx \frac{1}{2} \ln \frac{W^2}{m_P^2} \tag{49}$$

$$y_X = \tfrac{1}{2} \ln \tfrac{E_X + p_L}{E_X - p_L} \approx -\frac{1}{2} \ln \frac{W^2}{M_X^2} \tag{50}$$

Consequentially, the rapidity gap between the proton and system X is:

$$\Delta y = y_P - y_X \approx \ln \frac{W^2}{m_P M_X} \tag{51}$$

For typical values $W = 200\,\mathrm{GeV}$ and $M_X = 20\,\mathrm{GeV}$ we get for the rapidity gap $\Delta y \approx 7.7$. But the system X dissociates into hadrons that will span into some region of $\Delta y \sim \ln M_X \approx 3$. So we can conclude that the separation between the proton and fragments of the X system will be in this case at least 4 units of rapidity. In the general case, this value can be smaller than 4, but still a rapidity gap of $\Delta y > 2$ is observed.

3.2 Proton Dissociation

There are also processes, where the outgoing proton does not remain intact and also dissociates into some system Y,

$$\gamma^* \; p \quad \xrightarrow{I\!P} \quad X \; Y. \tag{52}$$

This type of events corresponds to *diffractive double dissociation* (see fig. 6). If the Y system has low mass then a LRG between X and Y systems is still observed. Very often it is impossible to determine exactly whether proton dissociation occurred or not. Some constraints on M_Y can be set, and are presented in the next paragraph.

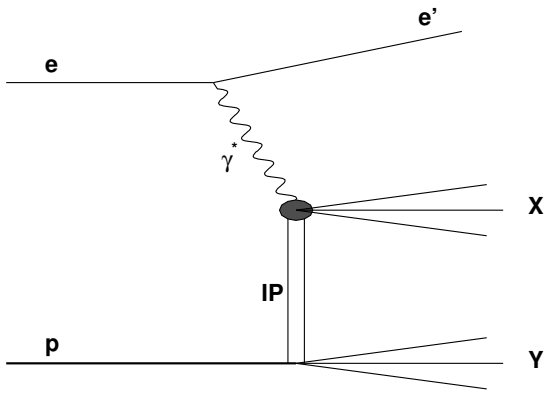

Figure 6: *Typical diffractive double dissociation event at HERA.*

If the proton broke up then one cannot be sure that the exchanged object had vacuum quantum numbers. In addition a simple description of the proton-Pomeron vertex is no longer correct.

To get a pure sample for the study of the partonic structure of the Pomeron it is necessary to exclude proton dissociation events. Sometimes the selection is obvious - when you see in the detector remnants of the system Y, but there are cases when M_Y and t are so small that the outgoing proton or the Y system cannot be seen in the detector. In the latter case, appropriate corrections must be made.

3.3 HERA data

Our study is based on the experimental results of $x_{I\!P} F_2^{D(3)}$ which were obtained by the H1 and the ZEUS experiments, running at the HERA collider. In order to obtain the diffractive cross section, an initial selection of diffractive events must be done. Different experimental groups use different techniques to select diffractive events. There are three methods used at HERA. events. One [13] uses the Leading Proton Spectrometer (LPS) to detect the scattered proton and by choosing the kinematic region where the scattered proton looses very little of its initial longitudinal energy, it ensures that the event was diffractive. A second method [12] simply requests a large rapidity gap (LRG) in the event and fits the data to contributions coming from Pomeron and Reggeon exchange. The third method [11] uses the distribution of the mass of the hadronic system seen in the detector, M_X, to isolate diffractive events. We will refer to these three as ZEUS LPS, H1 and ZEUS FPC methods, respectively. The data obtained using these methods were treated independently.

The diffractive structure function and the kinematic range each method covers, are presented in the Appendix §9 as well as the figures 35 - 38 which show the kinematic range covered by the different experiments in $(Q^2 - x_{I\!P})$, $(Q^2 - x)$, $(Q^2 - \beta)$ and $(Q^2 - M_X)$ planes, correspondingly. Included in the Appendix §9 are tables 2, 3, 4 containing the measured diffractive structure functions obtained with each of the three methods.

In order to compare three approaches we must have in mind the following issues:

- The ZEUS LPS allows to measure the proton directly. However it has low geometrical acceptance which leads to a low statistics.

- In the case of ZEUS FPC and H1 methods the proton goes down the beam pipe and cannot be measured directly. In the latter case few difficulties appear.

    i. One cannot be sure that the proton, that went down the beam pipe, indeed remained intact and did not dissociate. Detector structure and kinematics provide only an upper limit for masses of the state that went down the beam pipe. For the H1 detector this value is 1.6 GeV while for the ZEUS detector it is 2.3 GeV. To overcome this problem appropriate corrections, based on some theoretical assumptions, must be introduced.

    ii. LRGs can be also observed for non-diffractive events. They are exponentially suppressed. For small values of M_X their contribu-

tion is negligible, but becomes important for large masses. Non-diffractive events must be removed from the diffractive sample.

iii. Some hadrons from the X system may also go down the beam pipe. In that case the observed rapidity gap and the reconstructed mass M_X are not correct. In order to avoid this problem the selection on the basis of the *visible* rapidity gap between final state hadrons and beam pipe must be done.

- The ZEUS LPS and H1 methods select events which also include some contributions coming from Reggeon exchanges [31]. These contributions can be removed by applying $x_{I\!P} < 0.01$ cut, as discussed in §4.1. The ZEUS FPC(*Mass Decomposition*) method which subtracts the exponentially suppressed large rapidity gap events, in principle removes the Reggeon contribution and is left only with the proton dissociative background. The latter can not be removed for masses below 2.3 GeV, which amount to about 30% of the selected diffractive events [11].

All the points mentioned above are handled by making appropriate cuts (§4). Thus the main difference arises from the difference in methods used by experimental groups in selecting diffractive events. Different sensitivity to the proton dissociation produces some incompatibility between the H1 and the ZEUS data.

The H1 and ZEUS FPC data do not contain many points with big value of $x_{I\!P}$ (See Fig. 35). The reason for this is the restriction on the rapidity gap. When the proton is not seen in the detector a minimal rapidity is required for the remains of the X system to identify a diffractive event.

One technical issue must also be mentioned. The H1 and the ZEUS LPS data are presented in bins of Q^2 and β, while the ZEUS FPC data are presented in bins of Q^2 and M_X.

4 Data Selection

To test our model we need to select the data appropriately. The model is supposed to describe single diffractive dissociation events with Pomeron exchange. This implies that certain cuts have to be applied to the data that is going to be tested by the model. Following paragraphs describe and justify cuts that are going to be used.

4.1 Cut on $x_{I\!P}$

As described in section §3.3, the selected events include contribution coming from Pomeron and Reggeon exchanges. In order to eliminate the region with significat Reggeon contribution, a cut on $x_{I\!P}$ is necessary. A study [31] of the contributions of different exchanges to the flux shows that a cut of $x_{I\!P} < 0.01$ ensures that the contribution of the Pomeron is dominant (see fig. 7). The

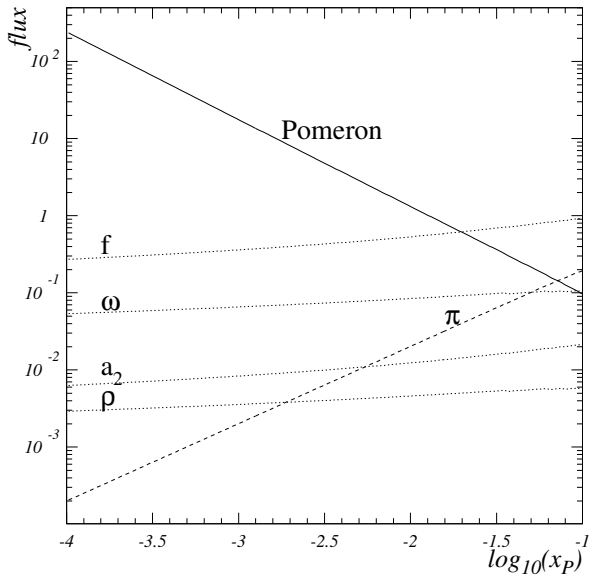

Figure 7: *The integrated over t flux factors of f_2, ω, a_2 and ρ Reggeons as a function of $x_{I\!P}$. For comparison we also present the Pomeron (solid) and pion (dashed) flux factors. Taken from [31].*

same study also ensures that for this cut the Pomeron exchange contribution to $x_{I\!P} F_2^{D(3)}$ is dominant (see fig. 8). Therefore our choice of the cut on $x_{I\!P}$ is,

$$x_{I\!P} < 0.01 \tag{53}$$

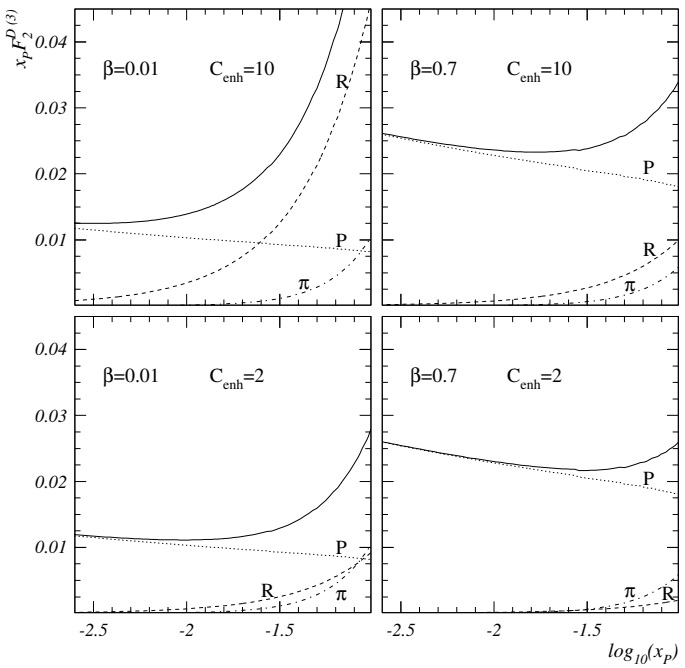

Figure 8: *The structure function* $x_{I\!P} \cdot F_2^{D(3)}(x_{I\!P}, \beta, Q^2)$ *as a function of* $x_{I\!P}$ *at* $Q^2 = 4\,\mathrm{GeV}^2$ *for two values* β *and two values of the ratio of the triple pomeron to pomeron-reggeon-reggeon couplings,* C_{enh}*. The Pomeron (*$I\!P$*), Reggeon (R) and pion (*π*) contributions to the total structure function (solid lines) are shown as seperate curves. Taken from [31].*

4.2 Cut on Q^2

An additional cut that we need to apply is the cut on the Q^2 value. We start the evolution at $Q^2_{ini} = 3\,\mathrm{GeV}^2$ and select events with $Q^2 > Q^2_{ini}$. The CTEQ package has difficulties with performing backward evolution. In addition, non-perturbative effects appear at small values of Q^2.

4.3 Cut on M_X

The M_X value represents the invariant mass of the X system (see Fig. 1). At small value of M_X, additional types of interactions take place. One of them is the vector meson production processes. For example ρ meson production dominates for diffractive events at $M_X \approx M_\rho = 0.77$ GeV. The theory used to describe such processes is different and thus we want to exclude this kind of data from our analysis. To achieve this we will apply a cut of $M_X > 2\,\mathrm{GeV}$ to leave out the range of light vector meson masses.

5 Regge Factorization test

The Regge Factorization assamption (§2.7) can be reduced to the following,

$$F_2^{D(4)}\left(x_{I\!P},\, t\,, \beta,\, Q^2\right) \;=\; f(x_{I\!P}, t) \cdot F(\beta, Q^2), \tag{54}$$

where $f(x_{I\!P}, t)$ represents the Pomeron flux which is assumed to be independent of β and Q^2 and $F(\beta, Q^2)$ represents the Pomeron structure and is β and Q^2 dependent. In order to test this assumption, we check whether the flux $f(x_{I\!P}, t)$ is indeed independent of β and Q^2 on the basis of the available experimental data.

To perform this we introduce a normalization factor $N(\beta, Q^2)$ that incorporates Q^2 and β dependence of the Pomeron structure function and is obtained from the fit. This allows us to test just the $x_{I\!P}$ behavior of $F_2^{D(3)}\left(x_{I\!P}\,, \beta,\, Q^2\right)$.

Two parameterizations were tested,

$$x_{I\!P} F_2^{D(3)}\left(x_{I\!P}\,, \beta,\, Q^2\right) \;=\; N(\beta, Q^2) \frac{1}{x_{I\!P}^A}, \tag{55}$$

$$x_{I\!P} F_2^{D(3)}\left(x_{I\!P}\,, \beta,\, Q^2\right) \;=\; N(\beta, Q^2) \int_{-1}^{0} dt f_{DL}(x_{I\!P},\, t)\,, \tag{56}$$

where $f_{DL}(x_{I\!P},\, t)$ is the Donnachie-Landshoff Pomeron flux factor (Eq. (40)). In the following sections we will study the Q^2 and β dependence of A and $\alpha_{I\!P}(0)$.

5.1 Test of Q^2 independence

Fits of the $x_{I\!P}$ dependence to the data sets were done in different Q^2 ranges as well as in the total $Q^2 > 3\,\mathrm{GeV}^2$ range. Additional kinematic cuts, used in the current work, were also applied such as $M_X > 2\,\mathrm{GeV}$ and $x_{I\!P} < 0.01$.

The results of the fits to the data are shown in figures 9-14. Figures 9,11 and 13 show results of parameterization (55) to the ZEUS FPC, ZEUS LPS and H1 data, respectively. Figures 10,12 and 14 show the corresponding fits to expression (56). In the figures the left plot shows the value of the variable A or $\alpha_{I\!P}(0)$, as obtained from the fit, as a function of Q^2 and the right one shows the $\chi^2/d.o.f$ values for the corresponding fits. The horizontal band in the figures represents the result of the global fit that covers the $Q^2 > 3\,\mathrm{GeV}^2$ range.

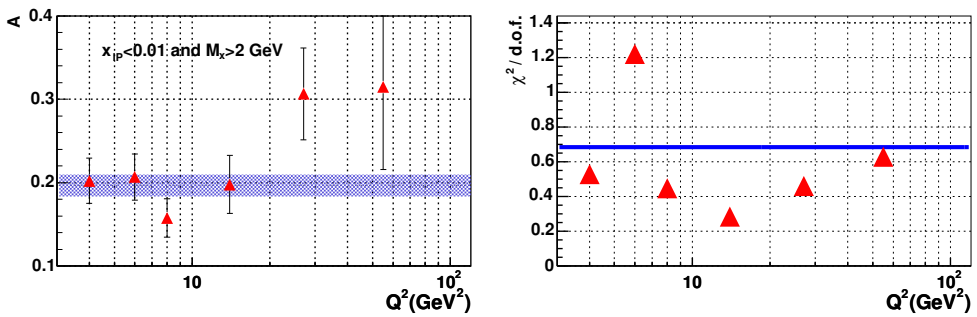

Figure 9: *The right plot shows values of A as a function of Q^2 for the ZEUS FPC data in the kinematic region $x_{I\!P} < 0.01$ and $M_X > 2\,\mathrm{GeV}$. In the left plot the quality of the fits is provided. The horizontal band corresponds to a fit over the whole Q^2 range.*

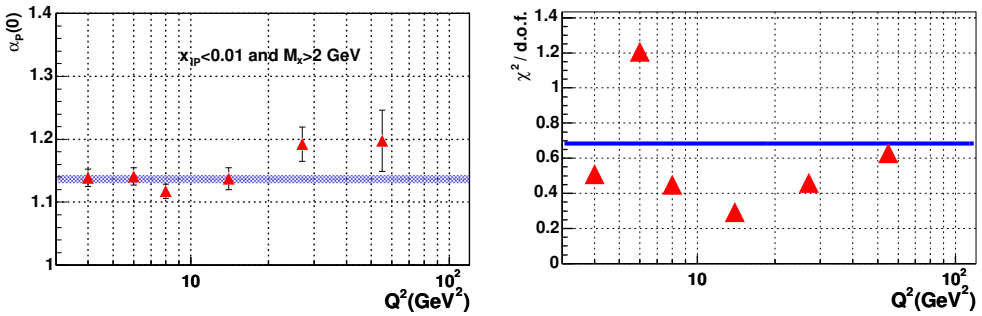

Figure 10: *The right plot shows values of $\alpha_{I\!P}(0)$ as a function of Q^2 for the ZEUS FPC data in the kinematic region $x_{I\!P} < 0.01$ and $M_X > 2\,\mathrm{GeV}$. In the left plot the quality of the fits is provided. The horizontal band corresponds to a fit over the whole Q^2 range.*

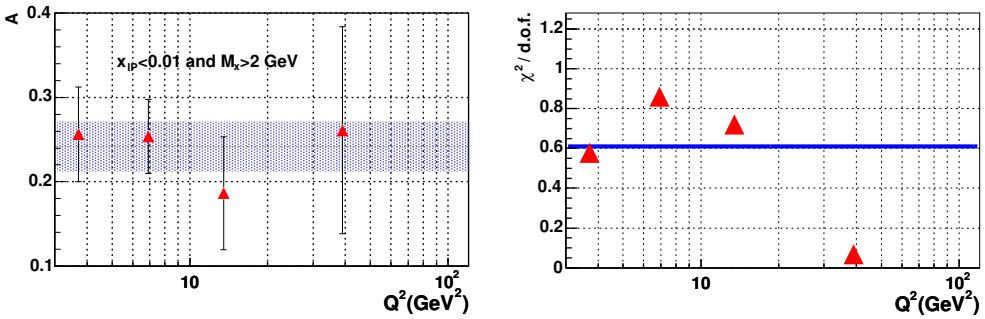

Figure 11: *The right plot shows values of A as a function of Q^2 for the ZEUS LPS data in the kinematic region $x_{I\!P} < 0.01$ and $M_X > 2\,\mathrm{GeV}$. In the left plot the quality of the fits is provided. The horizontal band corresponds to a fit over the whole Q^2 range.*

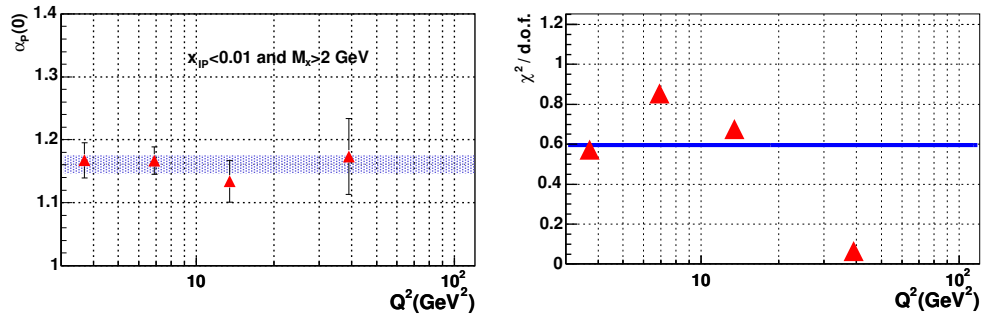

Figure 12: *The right plot shows values of $\alpha_{I\!P}(0)$ as a function of Q^2 for the ZEUS LPS data in the kinematic region $x_{I\!P} < 0.01$ and $M_X > 2\,\mathrm{GeV}$. In the left plot the quality of the fits is provided. The horizontal band corresponds to a fit over the whole Q^2 range.*

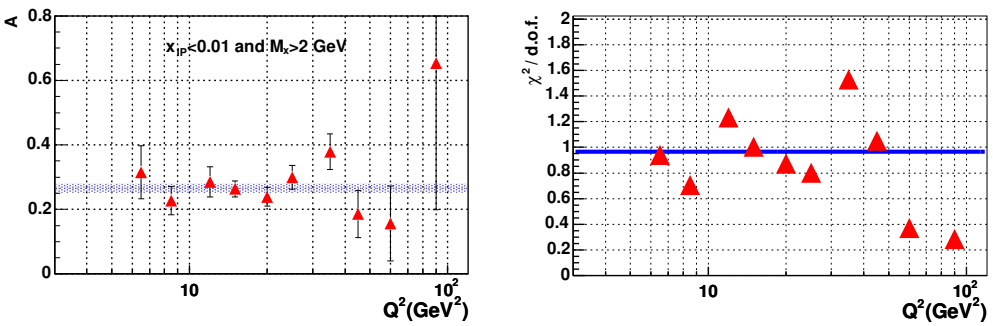

Figure 13: *The right plot shows values of A as a function of Q^2 for the H1 data in the kinematic region $x_{I\!P} < 0.01$ and $M_X > 2\,\mathrm{GeV}$. In the left plot the quality of the fits is provided. The horizontal band corresponds to a fit over the whole Q^2 range.*

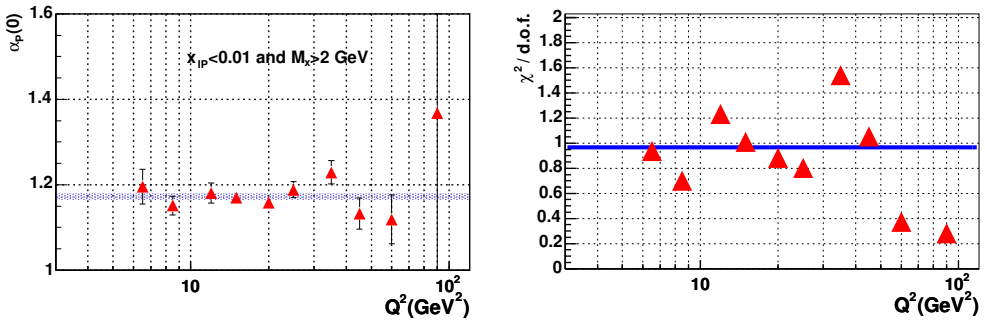

Figure 14: *The right plot shows values of $\alpha_{I\!P}(0)$ as a function of Q^2 for the H1 data in the kinematic region $x_{I\!P} < 0.01$ and $M_X > 2\,\mathrm{GeV}$. In the left plot the quality of the fits is provided. The horizontal band corresponds to a fit over the whole Q^2 range.*

One can see from the figures that the results obtained from the fits in different Q^2 ranges are compatible with the global fits. Some difference between the global fit and fits in the high Q^2 regions can be observed for ZEUS FPC data set (see figs. 9 and 10), but it still lies within 1.5 standard deviation range. From the small values of $\chi^2/d.o.f(\lesssim 1)$ follows that the fits have a good quality.

One can also notice that the behavior of both parameterization formulas is almost the same and so for testing the β dependence we provide results only for parameterization (55).

5.2 Test of β dependence

In this section, the β dependence of $\alpha_{I\!P}(0)$ and A is tested. Fits to the data sets were done in different β ranges as well as in the total β range. Fits were done once for $x_{I\!P} < 0.01$ and once for the bigger $x_{I\!P}$ range. Additional kinematic cuts used in the current work were also applied: $M_X > 2\,\mathrm{GeV}$ and $Q^2 > 3\,\mathrm{GeV}^2$. Fit results for the parameterization (55) for ZEUS FPC, ZEUS LPS and H1 data sets are shown in Figs.15, 16 and 17, respectively. The horizontal band in the figures represents the result of the global fit that covers the whole β range.

It can be easily seen from these plots that for the case of $x_{I\!P} < 0.01$ the results are β independent while for the bigger $x_{I\!P}$ range there is clear β dependence. This dependence is the outcome of the inclusion of the Reggeon contribution.

5.3 Conclusion of the factorization test

The results provided in §5.1 and §5.2 show that there are almost no Q^2 and β dependence of the Pomeron flux factor when applying the cuts: $Q^2 > 3\,\mathrm{GeV}^2$, $M_X > 2\,\mathrm{GeV}$ and $x_{I\!P} < 0.01$. This justifies the usage of Regge Factorization in the description of diffractive events.

One can also notice that the results for the H1 and the ZEUS LPS data are significantly higher than the results for ZEUS FPC data (see also fig. 18). It must be also mentioned that the value of $\alpha_{I\!P}(0)$ can be dependent on the $x_{I\!P}$ cut, as can be seen in fig. 18. As the value of $x_{I\!P}$ increases above 0.01 the increasing contribution of the Reggeon decreases the value of $\alpha_{I\!P}(0)$.

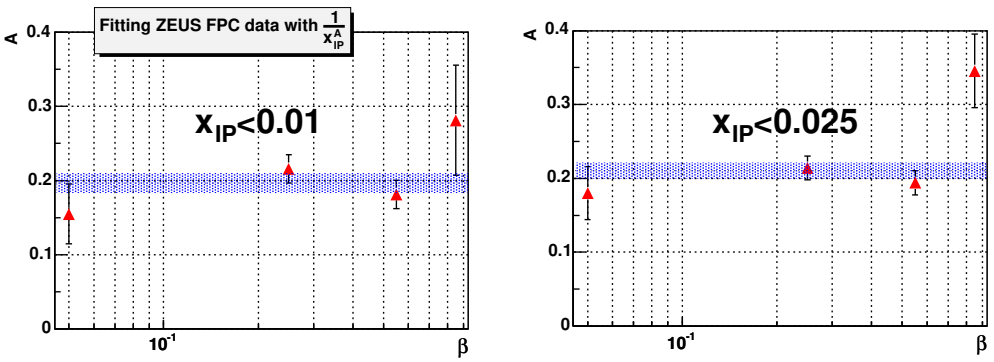

Figure 15: *The plots show values of A as a function of β for the ZEUS FPC data. The kinematic region is $M_X > 2\,\mathrm{GeV}$ and $Q^2 > 3\,\mathrm{GeV}^2$ for both plots. For the left plot the $x_{I\!P} < 0.01$ cut is applied, while for the right plot the cut is $x_{I\!P} < 0.025$. The horizontal band corresponds to a fit over the whole β range.*

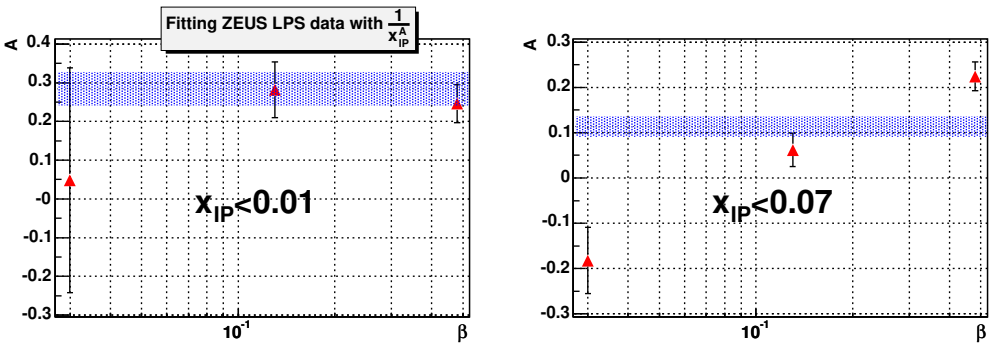

Figure 16: *The plots show values of A as a function of β for the ZEUS LPS data. The kinematic region is $M_X > 2\,\mathrm{GeV}$ and $Q^2 > 3\,\mathrm{GeV}^2$ for both plots. For the left plot the $x_{I\!P} < 0.01$ cut is applied, while for the right plot the cut is $x_{I\!P} < 0.07$. The horizontal band corresponds to a fit over the whole β range.*

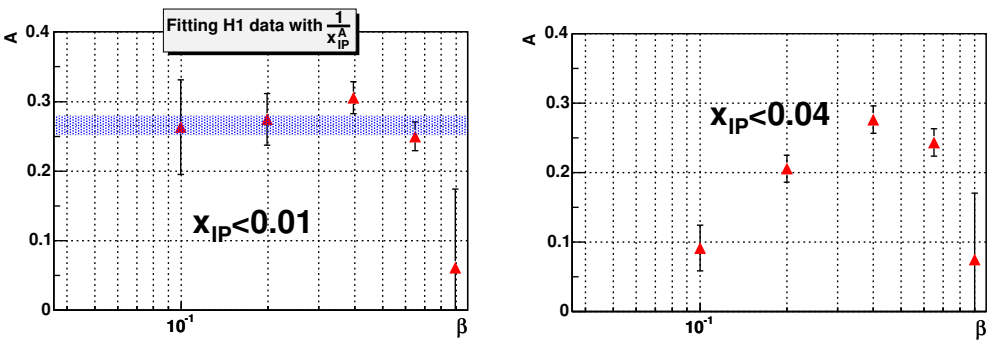

Figure 17: *The plots show values of A as a function of β for the H1 data. The kinematic region is $M_X > 2\,\mathrm{GeV}$ and $Q^2 > 3\,\mathrm{GeV}^2$ for both plots. For the left plot the $x_{I\!P} < 0.01$ cut is applied, while for the right plot the cut is $x_{I\!P} < 0.04$. The horizontal band in the left plot corresponds to a fit over the whole β range. For the $x_{I\!P} < 0.04$ the global fit failed and thus is not shown.*

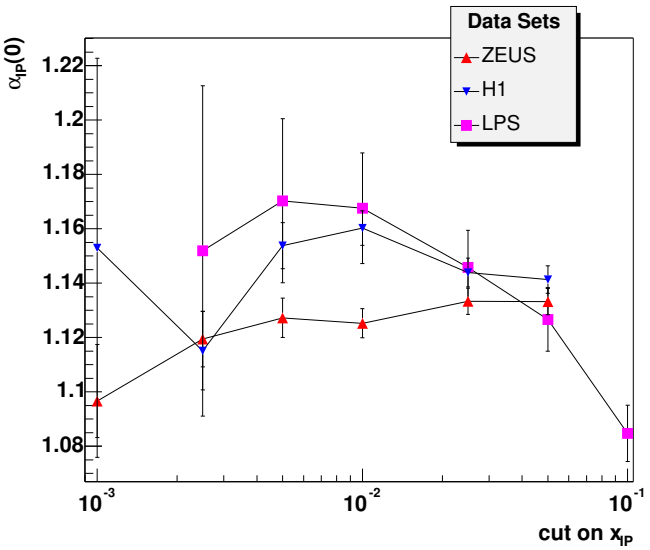

Figure 18: *Value of $\alpha_{I\!P}$ from the fit as a function of a cut on $x_{I\!P}$ for different data sets.*

6 Computations

This work contained a lot of numerical analysis, which makes use of different software packages.

- The *ROOT* package was chosen as a general framework.
- The *CTEQ* package was used for the QCD calculations.
- The *Minuit* package was used for fitting and minimization.

There are also some other packages that can be used in QCD computations. One of them is the QCDNUM package developed by M.A.J.Botje [29].

In §6.1 a comparison of the QCDNUM and the CTEQ packages will be presented. Then in §6.2, the fitting procedure will be described. Finally in §6.3 an outline of the calculations will be provided.

6.1 Comparison of QCDNUM and CTEQ packages

In both packages we consider-next-to-leading-order (NLO) calculations. One difference comes up in the calculation of the strong coupling constant α_S. QCD theory provides NLO differential evolution equation for α_S,

$$\frac{\partial a_S(\mu^2)}{\partial \ln \mu} = -\beta_0 a_S^2(\mu^2) - \beta_1 a_S^3(\mu^2), \tag{57}$$

where $a_S \equiv \alpha_S/4\pi$ and the beta functions are given by $\beta_0 = 11 - 2f/3$ and $\beta_1 = 102 - 38f/3$ with f the number of active flavors.

QCDNUM and CTEQ use different approaches to get approximate solution of this equation. CTEQ uses the Λ scheme where Λ_f is some QCD scale parameter which is different for different number of effective quarks. In this scheme α_S can be written as,

$$\alpha_S = \frac{4\pi}{\beta_0 \ln \frac{\mu^2}{\Lambda_f^2}} \left(1 - \frac{\beta_1 \ln \left(\ln \frac{\mu^2}{\Lambda_f^2} \right)}{\beta_0 \ln \frac{\mu^2}{\Lambda_f^2}} \right). \tag{58}$$

Λ_f values are chosen in such a way as to get a continuous α_S, when crossing thresholds for heavy flavors. The CTEQ package makes use of additional variable, N_{FL}, which denotes the total number of active quark flavors.

The QCDNUM package proceeds in a different way. It parameterizes α_S at some input scale μ_0 (which is often taken as M_Z) and then solves iteratively Eq. (59).

$$\frac{1}{a_S(\mu^2)} = \frac{1}{a_S(\mu_0^2)} + \beta_0 \ln \frac{\mu^2}{\mu_0^2} - \frac{\beta_1}{\beta_0} \ln \left(\frac{a_S(\mu^2)[\beta_0 + \beta_1 a_S(\mu_0^2)]}{a_S(\mu_0^2)[\beta_0 + \beta_1 a_S(\mu^2)]} \right) \tag{59}$$

Special treatment is done if the number of active quark flavors at the required scale μ is different from one at the input scale μ_0. The difference in α_S calculations as a function of Q^2 at different values of N_{FL} and $\Lambda_3$is shown in the Fig. 19. One can learn from this figure that there is certain disagreement

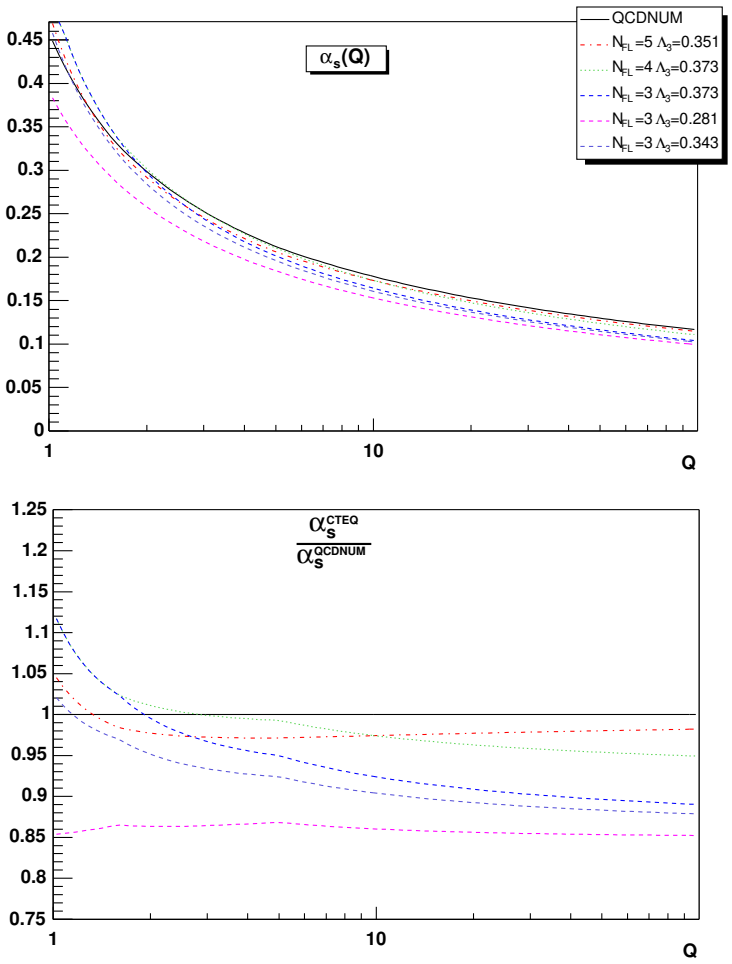

Figure 19: *Comparison of the value of the strong coupling constant α_S calculated by CTEQ and QCDNUM at different values of Λ_3 and N_{FL} as a function of Q.*

between two packages of about $3-5\%$ in the best case of $N_{FL}=5$ and $\Lambda_3 = 0.351$. The latter set of CTEQ parameters is used in future calculations.

Both packages perform the evolution of parton distributions using calculations over a $x-Q^2$ *grid*. The influence of the grid size in x, N_X, on the parton distribution functions at different values of Q^2 and β (equivalent to

x for the Pomeron case) is shown in Figs 20 and 21.

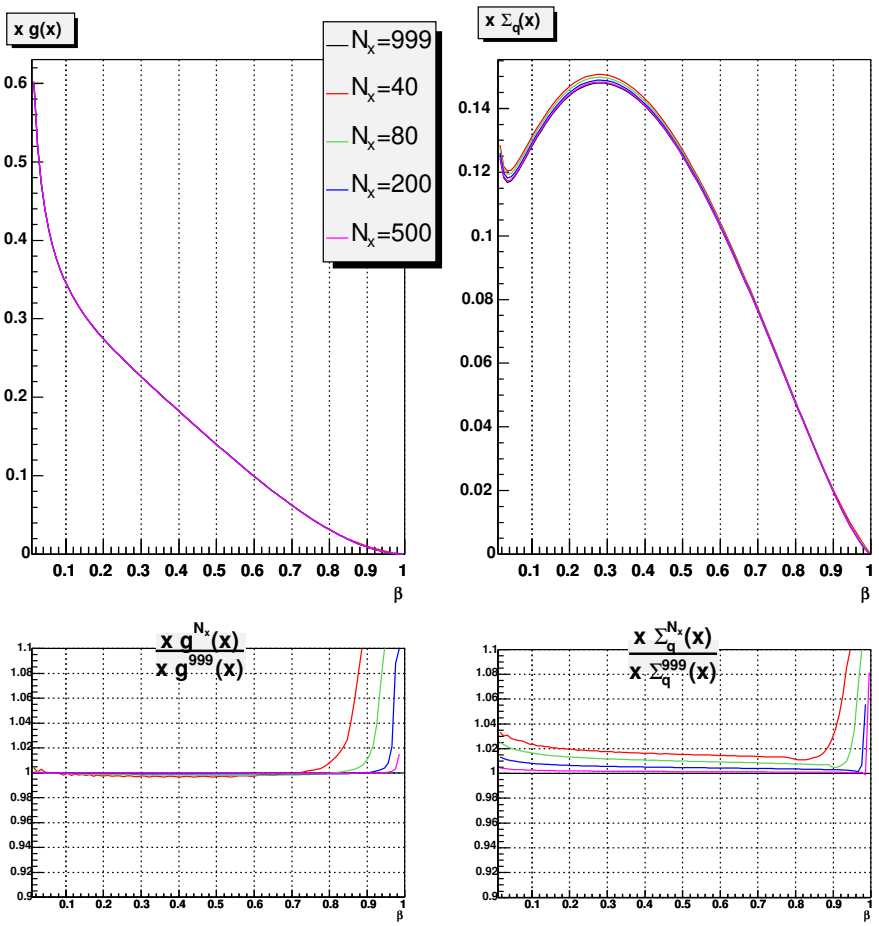

Figure 20: *Results of the evolution of the gluons, $xg(x)$, and the singlet distribution, $x\Sigma_q(x)$, from an initial scale of $Q_{ini} = \sqrt{3}\,\mathrm{GeV}$ to $Q = 10\,\mathrm{GeV}$, for different values of the grid size (N_X) as a function of β.*

In the current analysis $N_X = 80$ is used. One can see from the figures that an increase of the grid size changes the results, in the kinematic range, $0.01 \leq \beta \leq 0.9$ and $3\,\mathrm{GeV}^2 \leq Q^2 \leq 200\,\mathrm{GeV}^2$, up to 3%, but it also increases a lot the computation time.

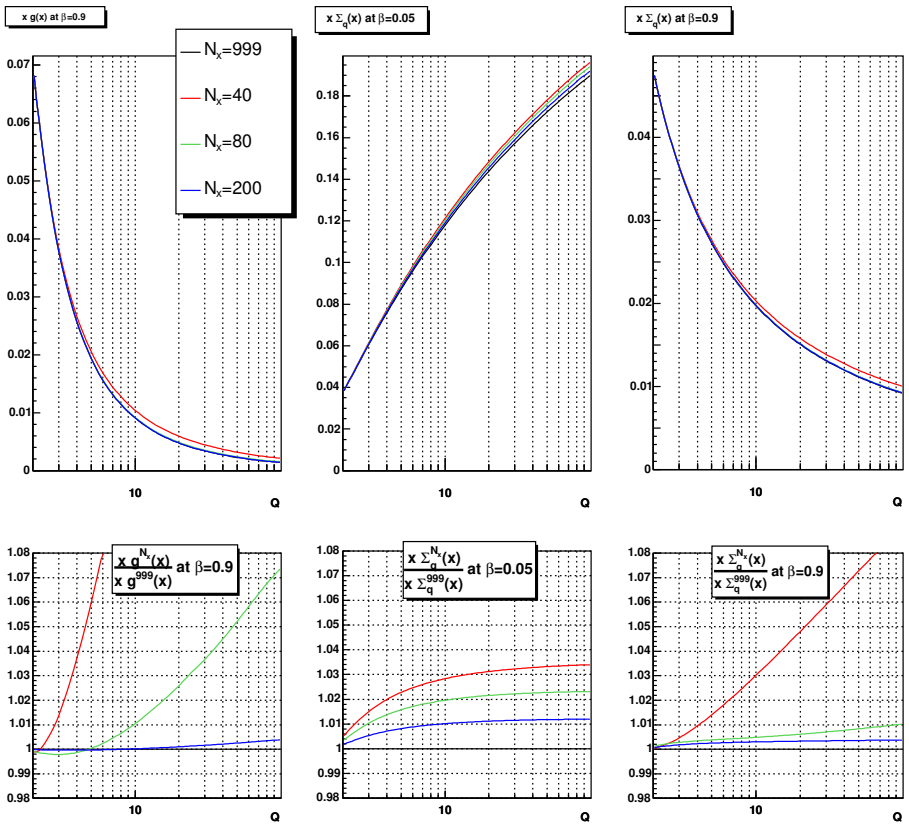

Figure 21: *Results of the evolution of the gluons, $xg(x)$, and the singlet distribution, $x\Sigma_q(x)$, from an initial scale of $Q_{ini} = \sqrt{3}\,\mathrm{GeV}$ for different values of the grid size (N_X) and for different β, as a function of $Q(\,\mathrm{GeV})$.*

6.2 Fitting proceedure

In the current work the experimental data were fitted by parameterized theoretical function. The best set of parameters was obtained by minimizing the total χ^2 using the *Minuit* package. Systematic errors were assumed to be uncorrelated and were included in the following way:

$$\Delta_{syst} = \frac{1}{2}(\Delta^{+}_{syst} + \Delta^{-}_{syst}) \;, \tag{60}$$

$$\Delta^2 = \Delta^2_{stat} + \Delta^2_{syst} \;. \tag{61}$$

The Minuit package also provides information about errors of the parameters. In the χ^2 method, in the case of uncorrelated parameters, their errors correspond to an increase of the χ^2_{min} value by one unit,

$$\chi^2(p_i + \Delta p_i) = \chi^2_{min} + 1, \tag{62}$$

where χ^2_{min} is the minimal χ^2 value obtained after minimization, p_i is the best value of parameter i and Δp_i is its error. In the case of correlated errors, the *error matrix* $V_{\lambda\mu}$ must be introduced. It is defined in the following way [30]:

$$M_{\lambda\mu} = \frac{1}{2}\frac{\partial^2\chi^2}{\partial p_\lambda \partial p_\mu} \tag{63}$$

$$V = M^{-1} \tag{64}$$

Then the error on any function F of the parameters p is, to first order, given by

$$(\Delta F)^2 = \sum_\lambda \sum_\mu \frac{\partial F}{\partial p_\lambda} V_{\lambda\mu} \frac{\partial F}{\partial p_\mu} \ . \tag{65}$$

Eq. (65) is used to calculate error bands of the results. The appropriate derivatives are obtained using the finite difference method.

6.3 Outline of the calculations

In our calculations we will proceed as follows:

1. Take the experimental measurements of diffractive structure function. Although they are often called $x_{I\!P} F_2^{D(3)}$, they actually correspond to $x_{I\!P}\sigma_r^{D(3)}$ (see Eq. (27)).

2. Use *QCD factorization* (§2.5) to define diffractive parton distribution functions.

3. Use *Regge factorization* (§2.7) to define Pomeron parton distributions and flux factor.

4. Guess parameterized PDFs of the Pomeron at some Q^2_{ini}.

5. Evolve them to obtain distribution, for required Q^2 value.

6. Calculate the reduced differential cross section - $\sigma_r^{D(3)}\left(x_{I\!P}\,, \beta, Q^2\right)$.

7. Fit the result to the data to get the best values for the function parameters.

8. Use the obtained results to study the partonic structure of the Pomeron.

7 Fits

In the previous section we tested the validity of the Regge factorization and discussed different issues of data selection. In the current section fits to the experimental data will be presented.

We will parameterize parton distribution functions of the Pomeron at $Q^2_{ini} = 3\,\mathrm{GeV}^2$ in the following way:

$$\begin{aligned} xg(x) &= A_g\, x^{\alpha_g}(1-x)^{\beta_g}, && (66)\\ xq(x) &= xu(x) = x\bar{u}(x) = xd(x) = x\bar{d}(x) \\ &= A_q\, x^{\alpha_q}(1-x)^{\beta_q}, && (67)\\ xs(x) &= x\,\bar{s}(x) = sxq(x), && (68)\\ xb(x) &= x\bar{b}(x) = x\,t(x) = x\,\bar{t}(x) = 0. && (69) \end{aligned}$$

A_g, A_q are assumed to be positive, in order to obtain positive parton densities, and s was set to zero (see §2.8). The powers α_q, β_q, α_g and β_g must be bigger than -1 in order to have total parton momentum to converge. No additional constraints were applied on the parameters.

In the following chapters results of the fits performed over the different data sets will be presented.

For each data set the following plots are provided:

- Fit curve including the error bands over the data points.
- Parton distribution functions of the Pomeron at different values of Q^2 as a function of β.
- Fraction of the Pomeron momentum carried by gluons.

7.1 Fit Results

Fits to ZEUS FPC, ZEUS LPS and H1 data were performed (see tables 2, 3 and 4 respectively). Data were selected according to the cut: $Q^2 > 3\,\mathrm{GeV}^2$, $x_{I\!P} < 0.01$ and $M_X > 2\,\mathrm{GeV}$.

In table 1 values of the parameters, as obtained from the fits for different data sets, are presented. General fit information including probability and χ^2, is also provided.

7.2 Fit presentation

The results of the fits from Table 1 are shown in Figs 22 - 26.

Table 1: Fit results for different data sets

Name	ZEUS FPC	ZEUS LPS	H1
$\alpha_{I\!P}(0)$	1.138 ± 0.011	1.189 ± 0.020	1.178 ± 0.007
A_q	0.107 ± 0.016	0.025 ± 0.007	0.092 ± 0.017
α_q	0.405 ± 0.021	0.19 ± 0.07	1.28 ± 0.07
β_q	0.103 ± 0.004	-0.396 ± 0.002	0.29 ± 0.03
A_g	6.09 ± 0.77	47 ± 27	0.191 ± 0.013
α_g	0.524 ± 0.036	1.23 ± 0.16	-0.639 ± 0.002
β_g	4.51 ± 0.07	12.8 ± 4.3	-0.87 ± 0.03
N_{points}	98	27	182
N_{params}	7	7	7
χ^2	90.7	10.1	189
$\chi^2/d.o.f.$	0.995	0.5	1.0
$Probability$	49%	96%	48%

Figs 22, 24 and 26 show the experimental data together with the corresponding fit results as a function of $x_{I\!P}$ and as a function of Q^2 for ZEUS FPC, ZEUS LPS and H1 data sets, respectively. Figs 23, 25 and 27 show the corresponding Pomeron parton distribution functions as a function of β for different values of Q^2.

One can see from the figures that the experimental data are described well by the corresponding fits. This can be also seen from the high probability values shown in table 1. It is worthwhile to mention that because of the large statistical errors and the limited β range of the data, we get big uncertainties in the ZEUS LPS fit results (see fig. 25).

Since we didn't impose any sum rule (see Eq. (38)) on the Pomeron parton distribution functions, the absolute value of these functions in not significant. However the behavior of these functions and their relation can be of interest. It must be mentioned that the initial behavior of pdfs is highly constrained by the chosen parameterization.

It can be seen from fig. 23 that the quark constituent of the Pomeron dominates at high β while gluons dominate at low β for the ZEUS FPC fit. For the H1 fit (fig. 27) we see the dominance of gluons in all the β range. In case of the ZEUS LPS fit (fig. 25) we also see the dominance of quarks at high β but we must remember that the ZEUS LPS sample does not contain data above $\beta > 0.47$ and thus the pdfs are not constrained in that region.

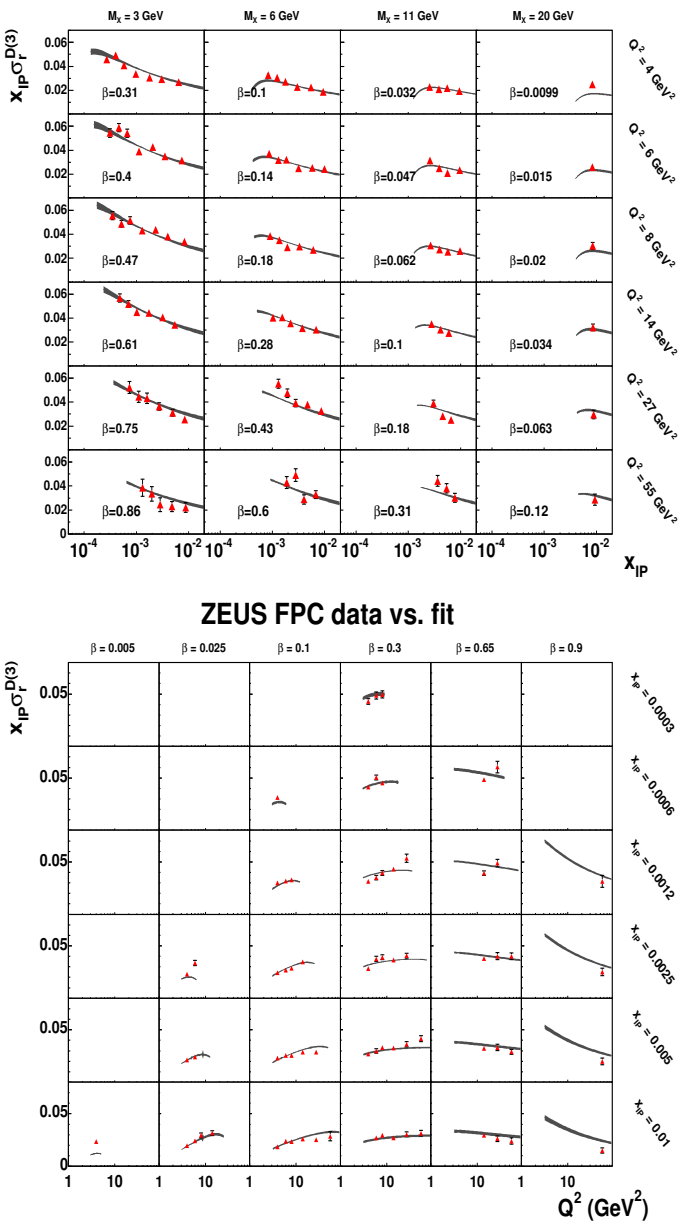

Figure 22: *The diffractive reduced cross section of the proton multiplied by* $x_{I\!P}$, $x_{I\!P}\sigma_r^{D(3)}$, *as a function of* $x_{I\!P}$ *(*Q^2*) for the ZEUS FPC data compared to the appropriate fit, in different bins of* Q^2 *(*$x_{I\!P}$*) and* β*, as indicated in the figure. The kinematic cut is* $x_{I\!P} < 0.01$, $M_x > 2\,\mathrm{GeV}$ *and* $Q^2 > 3\,\mathrm{GeV}^2$. *The bands are the results of the corresponding NLO QCD fit including uncertainties.*

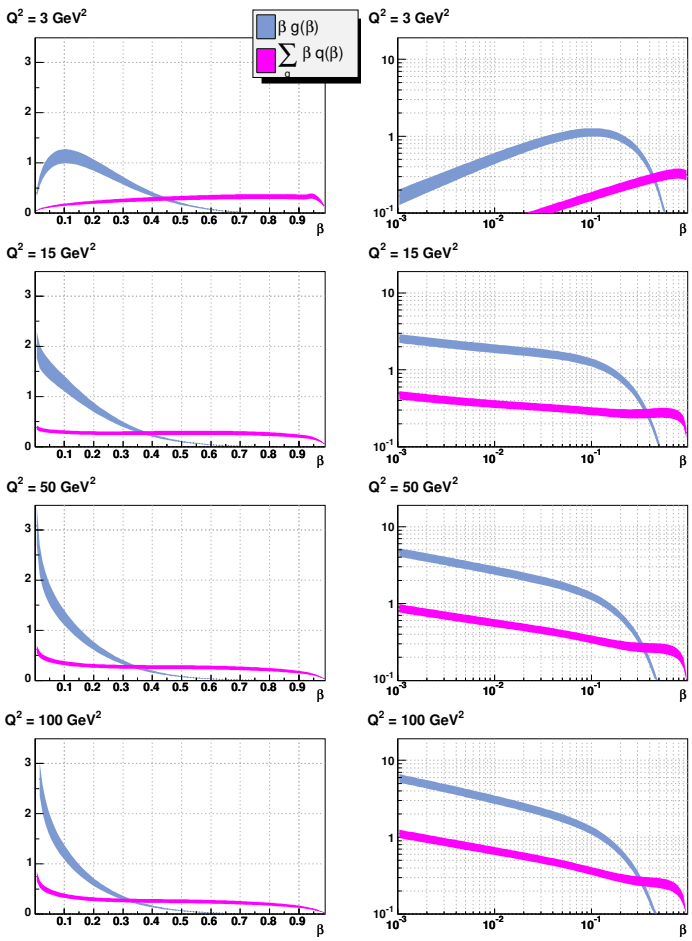

Figure 23: *Quark and gluon pdfs of the Pomeron as obtained from the ZEUS FPC data fit as a function of β, at different values of Q^2. Left plots present the results in linear and right plots in logarithmic scales.*

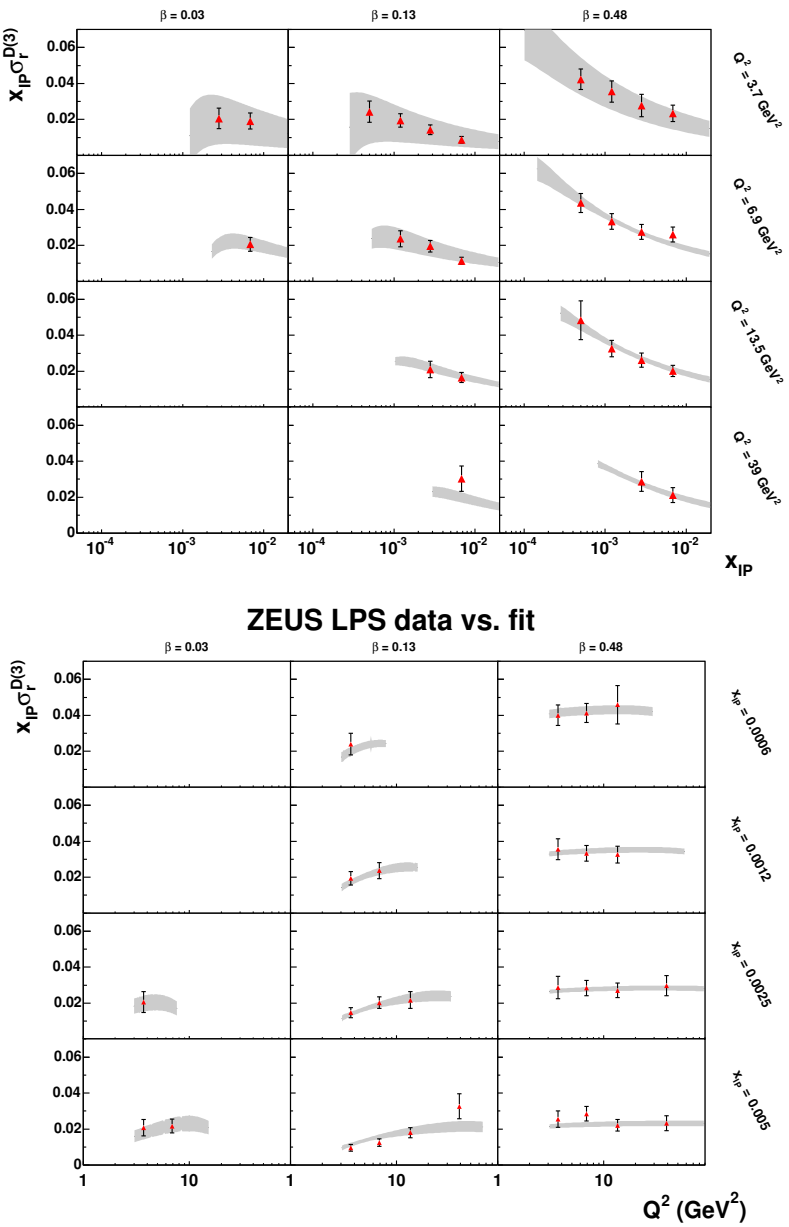

Figure 24: Same as Fig 22 but for the ZEUS LPS data set.

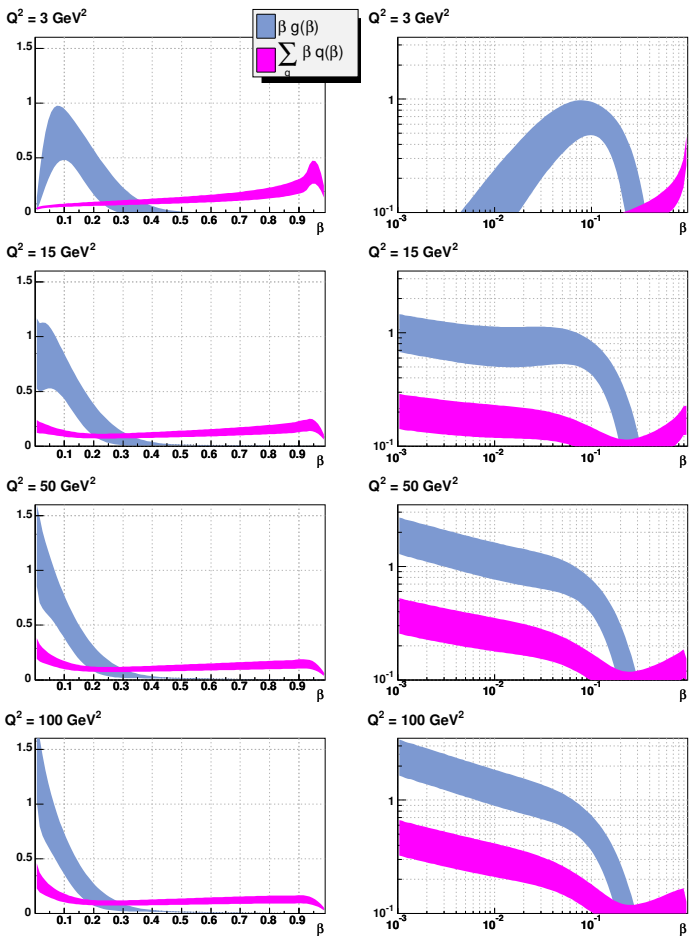

Figure 25: *Quark and gluon pdfs of the Pomeron as obtained from the ZEUS LPS data fit as a function of β, at different values of Q^2. Left plots present the results in linear and right plots in logarithmic scales.*

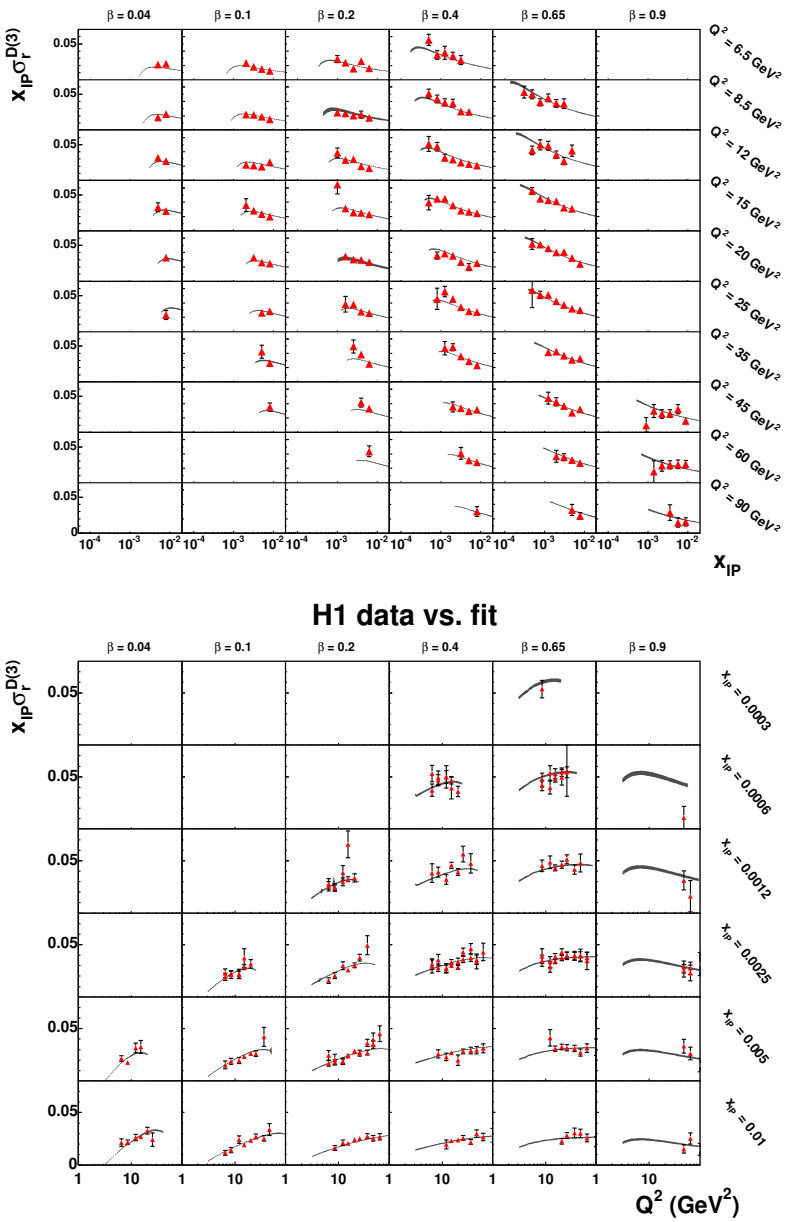

Figure 26: Same as Fig 22 but for the H1 data set.

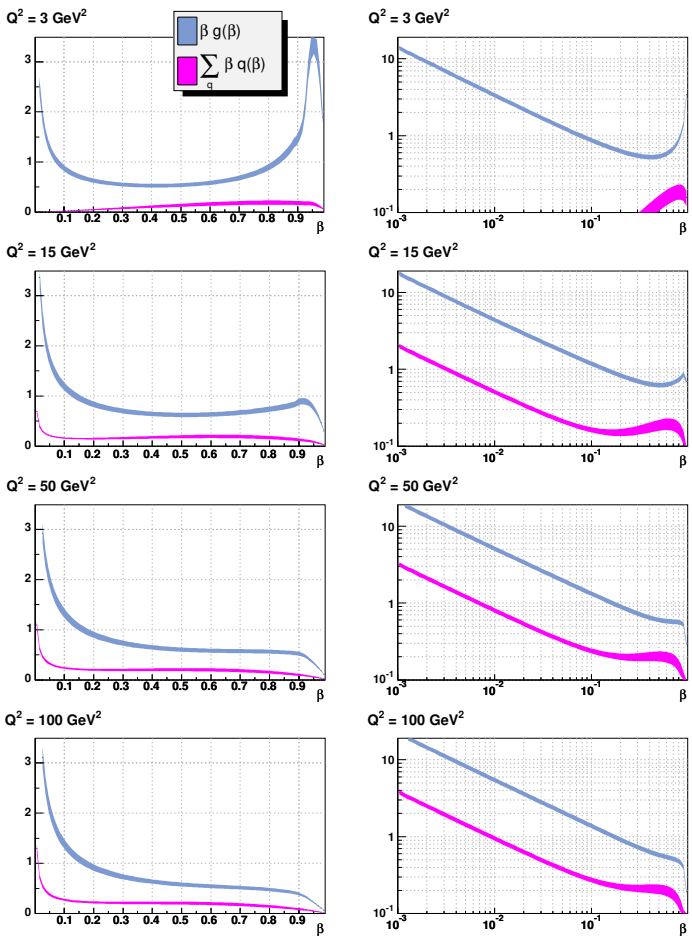

Figure 27: *Quark and gluon pdfs of the Pomeron as obtained from the H1 data fit as a function of β, at different values of Q^2. Left plots present the results in linear and right plots in logarithmic scales.*

It is worthwhile to mention that the second solution was found for this data set. It has higher value of χ^2 than the presented solution, but is also good with $\frac{\chi^2}{d.o.f.} < 1$. The values of $\alpha_{I\!P}(0)$ obtained from the different fits to the ZEUS LPS data are about the same, but the parton distribution functions appear to be different.

7.3 Comparison of the different fits

One way of checking the compatibility of all three data sets, is to make an overall fit to the whole data sample. Since the coverage of the β range in the ZEUS LPS data is limitted, we compare only the ZEUS FPC and H1 data.

A relative overall scaling factor was introduced to fix possible incompatibilities in the event selection. Unfortunately such a fit failed. Thus, the comparison between the data sets is done by using the fit results of one sample, plotted on the data of the other sample. This is presented in Figs 28 and 29.

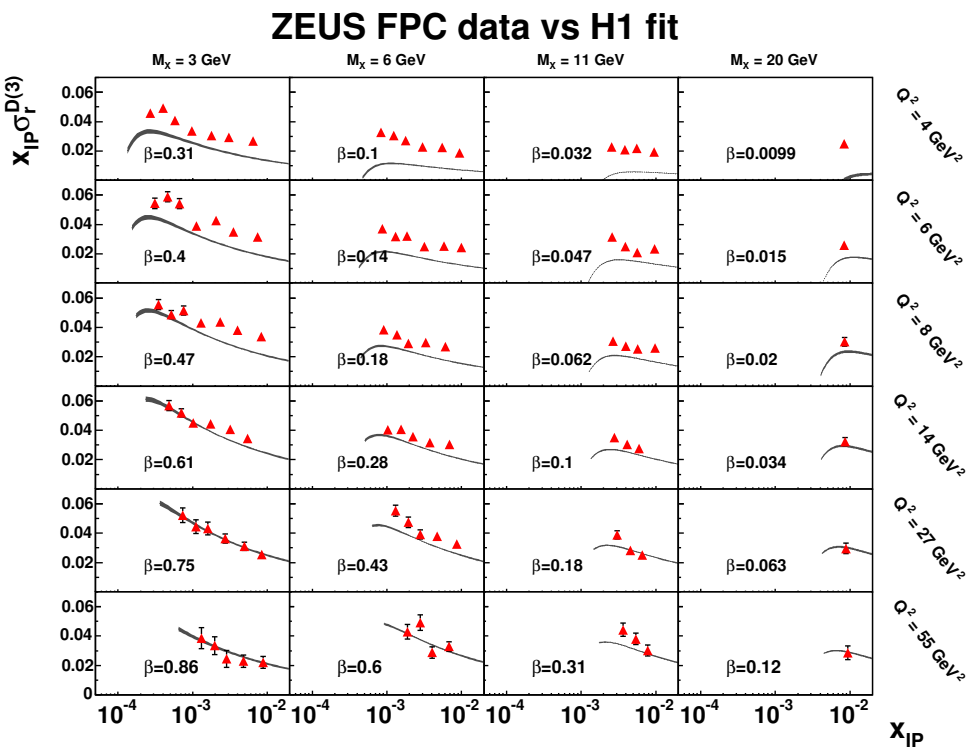

Figure 28: *The ZEUS FPC diffractive structure function data (triangles) as a function of $x_{I\!P}$, compared to the results of the H1 NLO QCD fit (band).*

Fig. 28 shows the H1 fit results compared to the ZEUS FPC data. The curves lie below the data points in the low Q^2 range, while at higher Q^2 values they seem to match the data. This seems to imply a different Q^2 behavior of the two data sets.

In fig. 29 the ZEUS FPC fit results are compared to the H1 data. No simple conclusion can be reached in this case; in some of the bins the curves lie above the data, while in others, they agree with the data points.

In conclusion we can state that there seems to be some incompatibility between the two data sets.

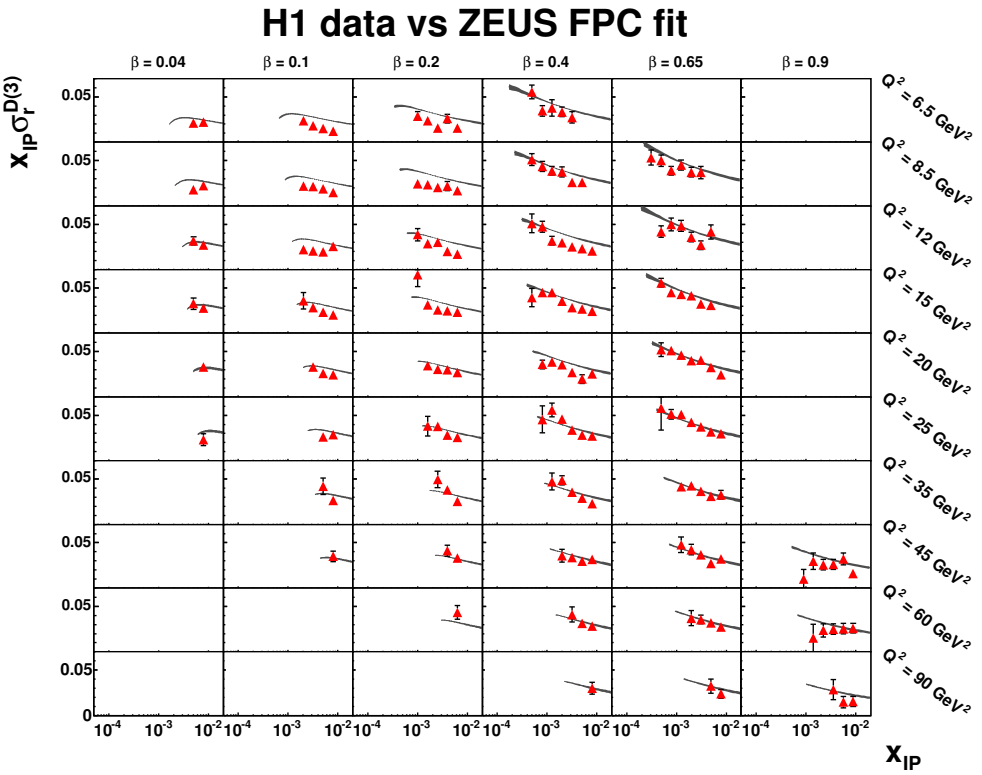

Figure 29: *The H1 diffractive structure function data (triangles) as a function of $x_{I\!P}$, compared to the results of the NLO QCD fit to the ZEUS FPC data (band).*

8 Results interpretation

In the current section some quantities, which can be calculated using the fit results, will be discussed.

8.1 Momentum carried by quarks and gluons

Using the fit results, the fraction of the Pomeron momentum carried by quarks and gluons can be calculated. It is defined in the following way:

$$P_q(Q^2) = \sum_i \int_0^1 d\beta\ \beta q_i(\beta, Q^2)\,, \tag{70}$$

$$P_g(Q^2) = \int_0^1 d\beta\ \beta q_i(\beta, Q^2)\,. \tag{71}$$

Since no momentum sum rule was imposed on the Pomeron, we normalize P_q and P_g in the following way:

$$\hat{P}_q = \frac{P_q}{P_q + P_g}, \tag{72}$$

$$\hat{P}_g = \frac{P_g}{P_q + P_g}. \tag{73}$$

The plots of $\hat{P}_q$ and $\hat{P}_g$ as a function of Q^2 are shown in Figs 30-32 for the ZEUS FPC, ZEUS LPS and H1 best fits, respectively. It can be seen from the figures that the gluons carry $55-65\%$ of the total Pomeron momentum for the ZEUS FPC fit. For the H1 fit this value is $80-90\%$ and for the ZEUS LPS fit gluon and quark parts are about the same with slight dominance of the first. In contrary to that, the second fit of the ZEUS LPS data, mentioned above, gives the results similar to the ones of H1 fit.

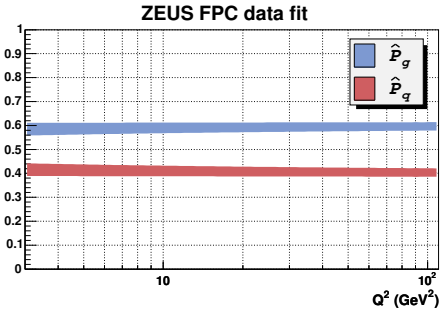

Figure 30: *Relative momentum fraction carried by gluons and quarks in the Pomeron as a function of Q^2, for the ZEUS FPC fit.*

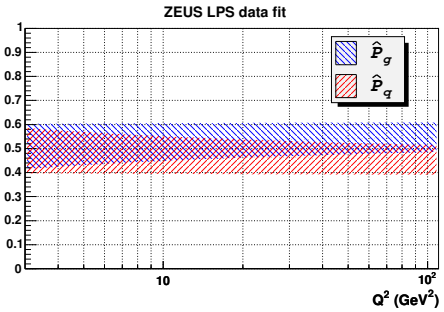

Figure 31: *Relative momentum fraction carried by gluons and quarks in the Pomeron as a function of Q^2, for the ZEUS LPS data.*

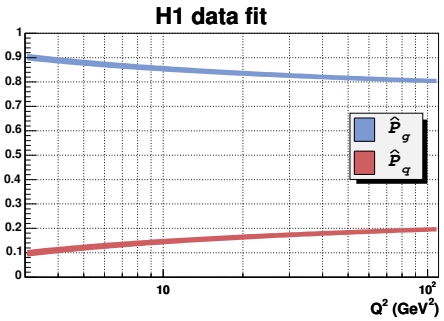

Figure 32: *Relative momentum fraction carried by gluons and quarks in the Pomeron as a function of Q^2, for the H1 data. ($Q^2 > 3\,\mathrm{GeV}^2$, $x_{I\!P} < 0.01$ and $M_X > 2\,\mathrm{GeV}$)*

8.2 Probability of diffraction

The probability that a certain parton is produced in a diffractive process is defined in Eq. (31). The following form was used in the computations:

$$P_g^D(x,Q^2) = \frac{\int_{x/0.01}^1 d\beta \, \frac{1}{\beta} f_{I\!P/P}(\frac{x}{\beta}) \, g^{I\!P}(\beta,Q^2)}{g^P(x,Q^2)} \, , \tag{74}$$

$$P_q^D(x,Q^2) = \frac{\sum_i \int_{x/0.01}^1 d\beta \, \frac{1}{\beta} f_{I\!P/P}(\frac{x}{\beta}) \, q_i^{I\!P}(\beta,Q^2)}{\sum_i q_i^P(x,Q^2)} \, , \tag{75}$$

where g^P and q_i^P are the gluon and the i-th quark distribution functions in the proton, $g^{I\!P}$ and $q_i^{I\!P}$ are the corresponding distribution functions in the Pomeron. The integration over β was preformed from $x/0.01$ to 1 which corresponds to the region of the single Pomeron exchange.

The probability of diffraction on quarks and gluons, as a function of x at different values of Q^2, is shown in Figs 33 and 34, using the results of the ZEUS FPC and the H1 data fits, respectively.

The ZEUS LPS data can not be used in this study because of the big uncertainties in the fit results. The ZEUS FPC data show that throughout the whole kinematic range shown in the figures, the probability for diffraction is not bigger than 0.15, far from the Pumplin [33] limit of 0.5. This is not the case for the H1 data. One can see that for small x the probability of diffraction on gluons for this data becomes greater than 0.5 which is unphysical. Please note that the results for $x < 2 \cdot 10^{-4}$ are in the region where H1 has no data. Thus the value of the probability of diffraction in that region is a prediction based on data lying in the upper region.

In order to get physical results, some processes must lower the expected value. One candidate for this might be gluon saturation [34] which could happen at small x.

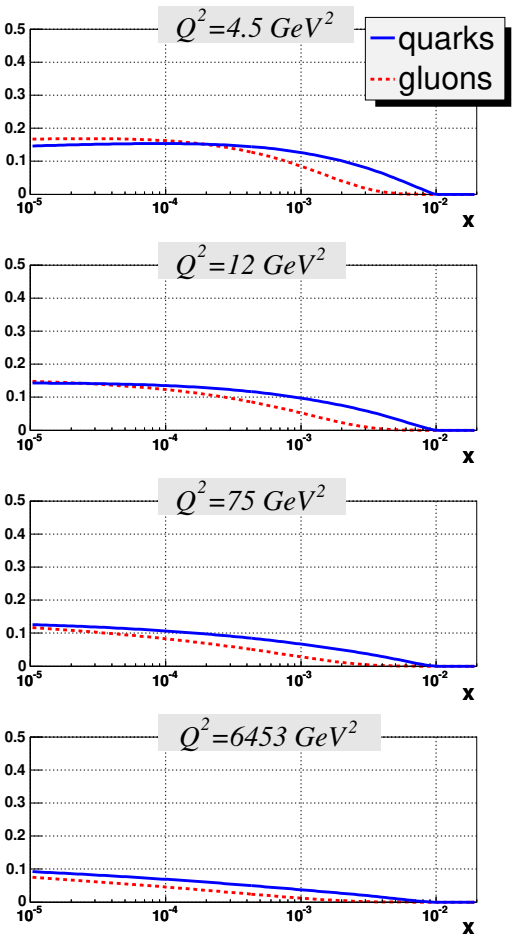

Figure 33: *Probability of diffraction as a function of x, at different values of Q^2, calculated from the results of the ZEUS FPC data fit.*

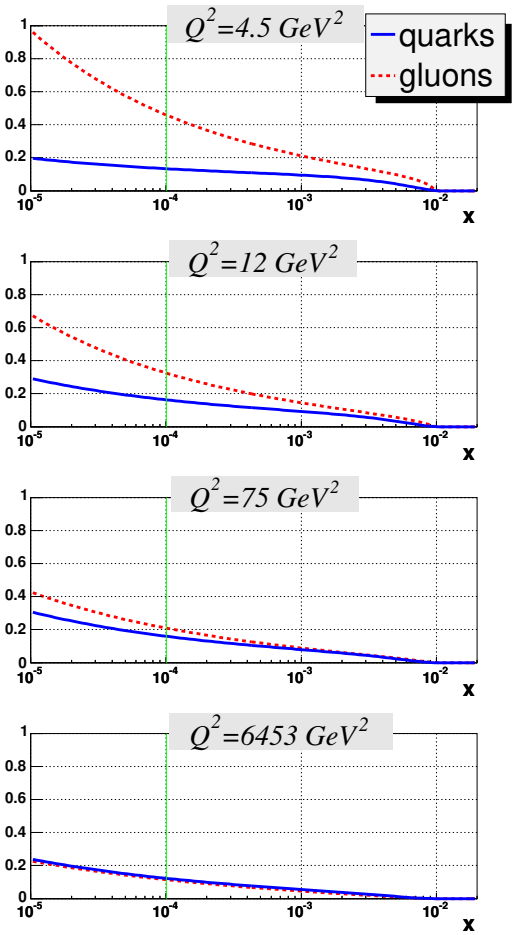

Figure 34: *Probability of diffraction as a function of x, at different values of Q^2, calculated from the results of the H1 data fit. The results of the fit below 10^{-4} are unphysical.*

9 Summary and Conclusions

In the present work the ZEUS FPC, ZEUS LPS and H1 data were used.

First, the Regge Factorization assumption was tested and was found to be consistent with available experimental data in the kinematic range: $M_X > 2\,\mathrm{GeV}$, $Q^2 > 3\,\mathrm{GeV}^2$ and $x_{I\!P} < 0.01$. It was also shown that the Regge factorization breaks when the $x_{I\!P} < 0.01$ cut is removed.

Next, the comparison of two numerical methods, CTEQ and QCDNUM, was done. It was shown that the results obtained by these methods may vary in up to 5%. In the current work the CTEQ method was used.

Then, NLO DGLAP fits to the inclusive diffractive data were done independently to the different data sets. The fits included the contribution of the longitudinal structure function, F_L^D. Simple parameterization of Pomeron parton distribution functions allowed to describe well the existing data in the selected kinematic range. The values obtained for $\alpha_{I\!P}(0)$ are,

$$\begin{aligned}
\alpha_{I\!P}(0) &= 1.138 \pm 0.011, \text{for the ZEUS FPC data,} \\
\alpha_{I\!P}(0) &= 1.189 \pm 0.020, \text{for the ZEUS LPS data,} \\
\alpha_{I\!P}(0) &= 1.178 \pm 0.007, \text{for the H1 data,}
\end{aligned}$$

These values are bigger than the ones obtained from hadron-hadron data, $\alpha_{I\!P}(0) = 1.09\pm...$ [32]. This implies a non-universal character of the Pomeron.

A comparison between the ZEUS FPC and the H1 data shows that they are incompatible in some of the kinematic region studied.

The fraction of the Pomeron momentum carried by gluons, extracted from the fit results, was found to be $70 - 90\%$ for the H1 and ZEUS LPS data, and $55 - 65\%$ for the ZEUS FPC data.

Additional quantity that was calculated was the probability of diffraction. Although it can be extrapolated to any region of x, the results for the H1 fit below 10^{-4} are unphysical. A possible reason for this is the onset of gluon saturation, which would invalidate the DGLAP evolution equations.

Acknowledgment

I am very grateful to my supervisors Prof. Halina Abramowicz and Prof. Aharon Levy for their help in the understanding of the subject and huge support in the analysis and the writing of this thesis.

I would like to thank Prof. John Collins, who hosted me in Penn. State University and directed me at the beginning of this study.

I appreciate a lot the help and support that I got from Dr. Arik Kreisler, Dr. Sergey Kananov, Dr. Zhenya Gurvich and their friendship. I am also thankful to my friends and office companions, Avi Mitrani and Ronen Ingbir and other members of our group in Tel-Aviv university.

Special thanks to Dr. Alexandr Proskuryakov who confirmed my results and guided me in DESY.

Additional thanks to the ZEUS and H1 people, who obtained the results that made this study possible.

This work was partially supported by the Israeli science foundation (ISF).

References

[1] P.D. Collins, "An Introduction To Regge Theory And High-Energy Physics," *Cambridge University Press, 1977.*

[2] V.N. Gribov, *JETP Lett.* **41** (1961) 667.

[3] S.J. Brodsky, L. Frankfurt, J.F. Gunion, A.H. Mueller, M. Strikman, "Diffractive Leptoproduction of Vector Mesons in QCD", *Phys. Rev.* **D50** (1994) 3134.

[4] H. Abramowicz, "Diffraction and the Pomeron", Int.J.Mod.Phys. **A15S1** (2000) 495.

[5] G. Ingelman and P. Schlein, *Phys. Lett.* **152B** (1985) 256.

[6] F.E. Low,*Phys. Rev.* **D12** (1975) 163,
S. Nussinov,*Phys. Rev. Lett.* **34** (1975) 1268.

[7] J.C. Collins, *Phys. Rev.* **D57** (2000) 3051; Erratum *ibid.* **D61** (2000) 019902; A. Berera and D.E. Soper, *Phys. Rev.* **D50** (1994) 4328; L. Trentadue and G. Veneziano, *Phys. Lett.* **B323** (1994) 201.

[8] ZEUS Collab., M. Derrick et al., *Phys. Lett.* **315** (193) 481; J. Breitweg et al., *Eur. Phys. J.* **C6** (1999) 43.

[9] H1 Collab., C. Adloff et al., *Zeit. Phys.* **C76** (1997) 613.

[10] ZEUS Collab., S. Chekanov et al., *Eur. Phys. J.* **C25** (2002) 169.

[11] ZEUS Collaboration,
"Deep Inelastic Diffractive Scattering with the ZEUS Forward Plug Calorimeter using 1998-1999 Data," DESY-04-131, hep-ex/0408009 (2004).

[12] H1 Collaboration,
"Measurement and NLO DGLAP QCD Interpretation of Diffractive Deep-Inelastic Scattering at HERA," paper 089 submitted to EPS 2003, Aachen.

[13] ZEUS Collaboration,
"Dissociation of virtual photons in events with a leading proton at HERA," DESY-04-131, hep-ex/0408009(2004).

[14] A. Donnachie and P.V. Landshoff,
Phys. Lett. **B296** (1992) 227, [hep-ph/9209205].

[15] A. Donnachie and P.V. Landshoff, *Nucl. Phys.* **B231** (1984) 189.

[16] A. Donnachie and P.V. Landshoff, *Nucl. Phys.* **B303** (1988) 634.

[17] V.N. Gribov and L.N. Lipatov, Yad. Fiz. **15** (1972) 1218.

[18] G. Altarelli and G. Parisi, *Nucl. Phys.* **B126** (1977) 298.

[19] Y.L. Dokshitzer, *Sov. Phys. JEPT* **46** (1977) 641.

[20] James D. Bjorken, *Hard diffraction and deep inelastic scattering*, Proceedings of DIS94, Eilat, Israel,(ed. A. Levy) p.151, 1994.

[21] K. Kang, J.R. Cudell, V.V. Ezhela, S.B. Lugovsky and N.P. Tkachenko, "Soft Pomeron and lower-trajectory intercepts," hep-ph/9812429, published in "Paris 1998, Quantum chromodynamics* 62-75"

[22] H. Abramowicz and A. Caldwell, "HERA collider physics" *Rev. Mod. Phys.* **71** (1999) 1275-1410,hep-ex/9903037

[23] J.C. Collins *Phys. Rev.* **D57** (1998) 3051,arXiv:hep-ph/9709499.

[24] J.C. Collins "Factorization in hard diffraction", J.Phys.G28(2002), 1069-1078, arXiv:hep-ph/0107252.

[25] L.Frankfurt and M.Strikman, "Future Small x physics with ep and eA Colliders", arXiv:hep-ph/9907221 3 Jul 1999.

[26] J. Collins, J. Huston, J. Pumplin, H. Weerts and J. Whitmore, "Measuring Parton densities in the Pomeron", *Phys. Rev.* **D51** (3182) 1995,arXiv:hep-ph/9406255.

[27] P.K. Malhotra and R. Orava, *Zeit. Phys.* **C17** (1983) 85.

[28] A.H. Mueller, *Phys. Rev.* **D2** (1970) 2963.

[29] M. Botje, "QCDNUM16: A fast QCD evolution program", *Zeus Note* **97-066**

[30] M. Botje, "Error propagation in QCD fits", Published in "Liverpool 2000, Deep inelastic scattering* 165-167" arXiv:hep-ph/0006193 16 Jun 2000.

[31] K. Golec-Biernat, J. Kwiecinski and A. Szczurek
"Reggeon and pion contributions in semi-exclusive diffractive processes at HERA" *Phys. Rev.* **D56** (1997) 3955,arXiv:hep-ph/9701254

[32] J.R. Cudell, K. Kang and S.K. Kim, "Bounds on the soft Pomeron Intercept", *Phys. Lett.* **B395** (1997) 311.

[33] J.Pumplin, *Phys. Rev.* **D8** (1973) 2899.

[34] K. Golec-Biernat and M. Würsthoff, *Phys. Rev.* **D59** (1999) 014017
K. Golec-Biernat and M. Würsthoff, *Phys. Rev.* **D60** (1999) 114023
K. Golec-Biernat and M. Würsthoff, *Eur. Phys. J.* **C20** (2001) 313

Appendix: Experimental data references

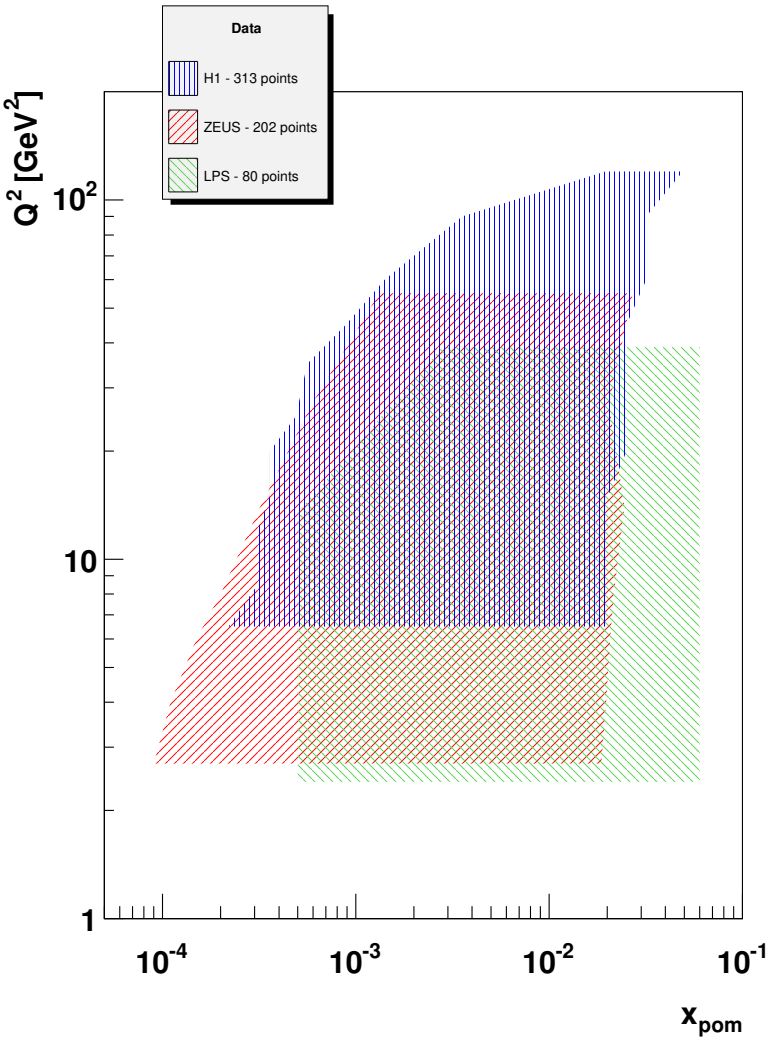

Figure 35: $Q^2 - x_{I\!P}$ *range covered by different experiments.*

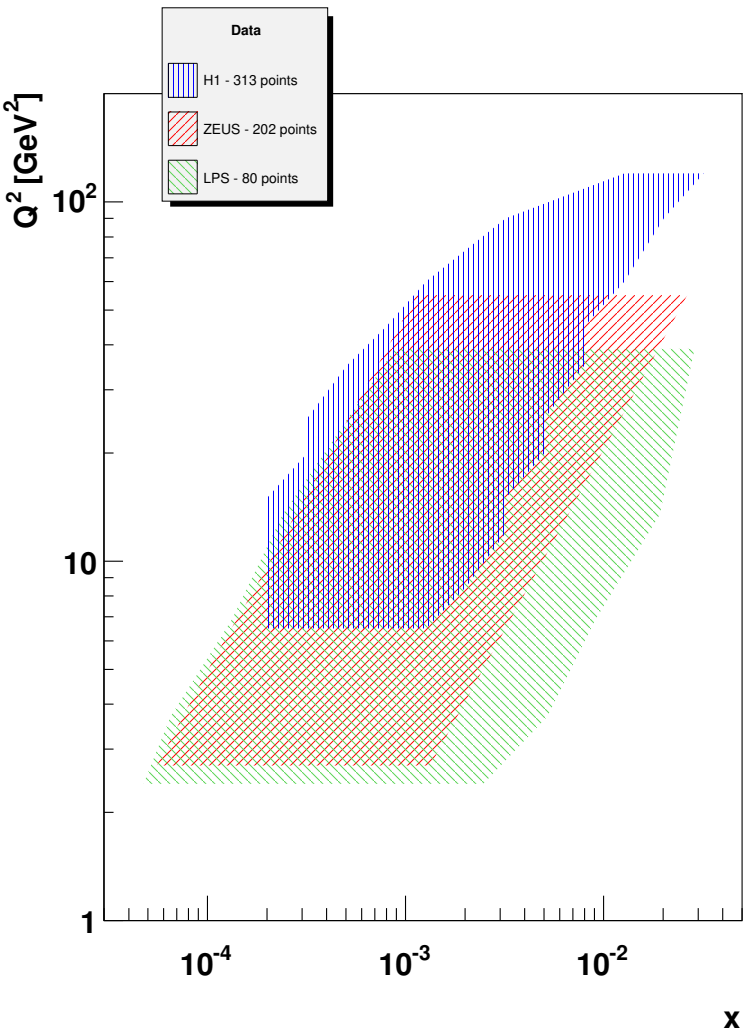

Figure 36: *$Q^2 - x$ range covered by different experiments.*

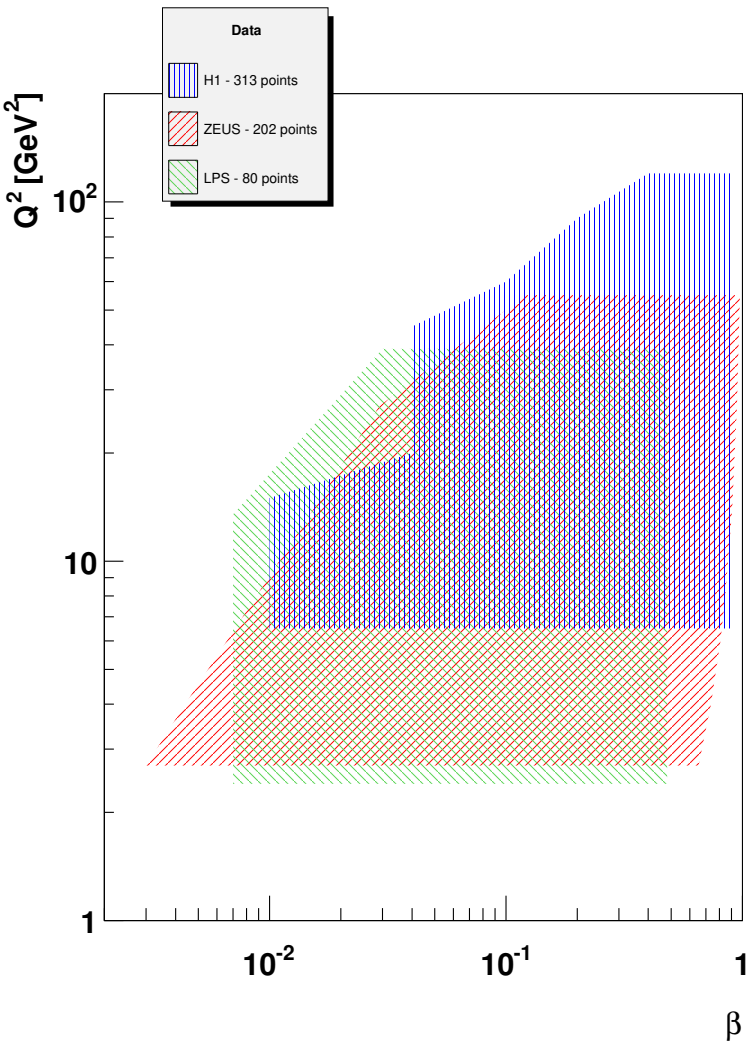

Figure 37: *$Q^2 - \beta$ range covered by different experiments.*

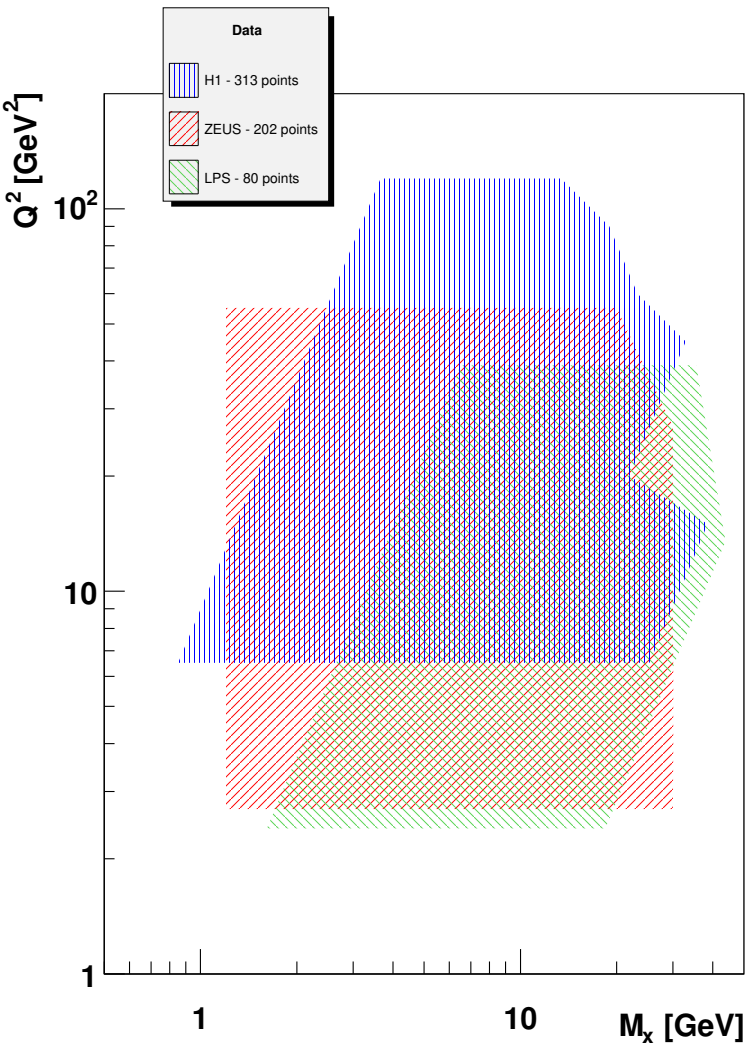

Figure 38: $Q^2 - M_X$ *range covered by different experiments.*

Table 2: ZEUS FPC diffractive data

$x_{I\!P}$	β	Q^2 (GeV^2)	$x_{I\!P}F_2^{D(3)}$	Δ_{stat}	Δ_{syst}
0.00204	0.6522	2.7	0.0340	± 0.0020	$^{+0.0048}_{-0.0030}$
0.00098	0.6522	2.7	0.0396	± 0.0024	$^{+0.0062}_{-0.0042}$
0.00057	0.6522	2.7	0.0416	± 0.0025	$^{+0.0036}_{-0.0033}$
0.00031	0.6522	2.7	0.0410	± 0.0021	$^{+0.0043}_{-0.0033}$
0.00018	0.6522	2.7	0.0433	± 0.0025	$^{+0.0046}_{-0.0048}$
0.00013	0.6522	2.7	0.0375	± 0.0024	$^{+0.0055}_{-0.0043}$
0.00009	0.6522	2.7	0.0400	± 0.0038	$^{+0.0098}_{-0.0074}$
0.00577	0.2308	2.7	0.0244	± 0.0018	$^{+0.0028}_{-0.0024}$
0.00277	0.2308	2.7	0.0234	± 0.0019	$^{+0.0012}_{-0.0018}$
0.00162	0.2308	2.7	0.0249	± 0.0018	$^{+0.0029}_{-0.0018}$
0.00088	0.2308	2.7	0.0283	± 0.0019	$^{+0.0020}_{-0.0021}$
0.00052	0.2308	2.7	0.0370	± 0.0026	$^{+0.0016}_{-0.0029}$
0.00036	0.2308	2.7	0.0393	± 0.0026	$^{+0.0018}_{-0.0048}$
0.00024	0.2308	2.7	0.0499	± 0.0035	$^{+0.0041}_{-0.0056}$
0.00915	0.0698	2.7	0.0177	± 0.0018	$^{+0.0011}_{-0.0011}$
0.00535	0.0698	2.7	0.0206	± 0.0018	$^{+0.0015}_{-0.0011}$
0.00293	0.0698	2.7	0.0226	± 0.0017	$^{+0.0026}_{-0.0021}$
0.00172	0.0698	2.7	0.0229	± 0.0019	$^{+0.0019}_{-0.0023}$
0.00119	0.0698	2.7	0.0252	± 0.0019	$^{+0.0018}_{-0.0024}$
0.00080	0.0698	2.7	0.0256	± 0.0020	$^{+0.0029}_{-0.0016}$
0.01711	0.0218	2.7	0.0170	± 0.0034	$^{+0.0035}_{-0.0015}$
0.00935	0.0218	2.7	0.0196	± 0.0021	$^{+0.0024}_{-0.0020}$
0.00550	0.0218	2.7	0.0170	± 0.0019	$^{+0.0024}_{-0.0016}$
0.00382	0.0218	2.7	0.0207	± 0.0019	$^{+0.0009}_{-0.0026}$
0.00256	0.0218	2.7	0.0212	± 0.0018	$^{+0.0026}_{-0.0007}$
0.01790	0.0067	2.7	0.0196	± 0.0056	$^{+0.0027}_{-0.0020}$
0.01243	0.0067	2.7	0.0164	± 0.0031	$^{+0.0024}_{-0.0015}$
0.00832	0.0067	2.7	0.0270	± 0.0030	$^{+0.0020}_{-0.0017}$
0.01865	0.0030	2.7	0.0233	± 0.0064	$^{+0.0042}_{-0.0028}$
0.00268	0.7353	4.0	0.0328	± 0.0014	$^{+0.0035}_{-0.0042}$
0.00129	0.7353	4.0	0.0356	± 0.0016	$^{+0.0048}_{-0.0049}$
0.00075	0.7353	4.0	0.0405	± 0.0018	$^{+0.0057}_{-0.0051}$
0.00041	0.7353	4.0	0.0469	± 0.0020	$^{+0.0051}_{-0.0043}$
0.00024	0.7353	4.0	0.0404	± 0.0020	$^{+0.0055}_{-0.0035}$
0.00017	0.7353	4.0	0.0503	± 0.0025	$^{+0.0042}_{-0.0053}$
0.00011	0.7353	4.0	0.0404	± 0.0027	$^{+0.0112}_{-0.0061}$
0.00641	0.3077	4.0	0.0269	± 0.0013	$^{+0.0022}_{-0.0013}$

Table 2: ZEUS FPC diffractive data (continued)

$x_{I\!P}$	β	$Q^2\,(\mathrm{GeV}^2)$	$x_{I\!P}F_2^{D(3)}$	Δ_{stat}	Δ_{syst}
0.00307	0.3077	4.0	0.0292	± 0.0015	$^{+0.0028}_{-0.0030}$
0.00180	0.3077	4.0	0.0304	± 0.0015	$^{+0.0024}_{-0.0029}$
0.00098	0.3077	4.0	0.0338	± 0.0016	$^{+0.0019}_{-0.0022}$
0.00058	0.3077	4.0	0.0407	± 0.0021	$^{+0.0039}_{-0.0023}$
0.00040	0.3077	4.0	0.0493	± 0.0024	$^{+0.0023}_{-0.0034}$
0.00027	0.3077	4.0	0.0459	± 0.0024	$^{+0.0022}_{-0.0046}$
0.01971	0.1000	4.0	0.0185	± 0.0028	$^{+0.0022}_{-0.0015}$
0.00946	0.1000	4.0	0.0187	± 0.0014	$^{+0.0021}_{-0.0017}$
0.00553	0.1000	4.0	0.0226	± 0.0014	$^{+0.0034}_{-0.0022}$
0.00302	0.1000	4.0	0.0227	± 0.0013	$^{+0.0012}_{-0.0020}$
0.00178	0.1000	4.0	0.0270	± 0.0017	$^{+0.0012}_{-0.0022}$
0.00123	0.1000	4.0	0.0304	± 0.0017	$^{+0.0021}_{-0.0015}$
0.00083	0.1000	4.0	0.0328	± 0.0018	$^{+0.0012}_{-0.0030}$
0.01729	0.0320	4.0	0.0145	± 0.0032	$^{+0.0025}_{-0.0025}$
0.00945	0.0320	4.0	0.0194	± 0.0019	$^{+0.0022}_{-0.0018}$
0.00556	0.0320	4.0	0.0219	± 0.0017	$^{+0.0014}_{-0.0024}$
0.00386	0.0320	4.0	0.0209	± 0.0014	$^{+0.0016}_{-0.0010}$
0.00258	0.0320	4.0	0.0227	± 0.0014	$^{+0.0009}_{-0.0015}$
0.01795	0.0099	4.0	0.0173	± 0.0051	$^{+0.0020}_{-0.0023}$
0.01247	0.0099	4.0	0.0206	± 0.0032	$^{+0.0025}_{-0.0021}$
0.00835	0.0099	4.0	0.0250	± 0.0024	$^{+0.0019}_{-0.0015}$
0.01868	0.0044	4.0	0.0228	± 0.0060	$^{+0.0034}_{-0.0030}$
0.00366	0.8065	6.0	0.0288	± 0.0019	$^{+0.0032}_{-0.0032}$
0.00176	0.8065	6.0	0.0328	± 0.0023	$^{+0.0072}_{-0.0031}$
0.00103	0.8065	6.0	0.0335	± 0.0022	$^{+0.0038}_{-0.0035}$
0.00056	0.8065	6.0	0.0367	± 0.0022	$^{+0.0038}_{-0.0045}$
0.00033	0.8065	6.0	0.0450	± 0.0030	$^{+0.0048}_{-0.0038}$
0.00023	0.8065	6.0	0.0393	± 0.0028	$^{+0.0058}_{-0.0023}$
0.00015	0.8065	6.0	0.0436	± 0.0036	$^{+0.0078}_{-0.0077}$
0.00739	0.4000	6.0	0.0314	± 0.0019	$^{+0.0027}_{-0.0034}$
0.00354	0.4000	6.0	0.0349	± 0.0023	$^{+0.0033}_{-0.0014}$
0.00207	0.4000	6.0	0.0426	± 0.0026	$^{+0.0030}_{-0.0030}$
0.00113	0.4000	6.0	0.0390	± 0.0022	$^{+0.0016}_{-0.0015}$
0.00067	0.4000	6.0	0.0542	± 0.0033	$^{+0.0011}_{-0.0029}$
0.00046	0.4000	6.0	0.0589	± 0.0035	$^{+0.0021}_{-0.0039}$
0.00031	0.4000	6.0	0.0544	± 0.0035	$^{+0.0022}_{-0.0037}$
0.02068	0.1429	6.0	0.0179	± 0.0031	$^{+0.0029}_{-0.0023}$

Table 2: ZEUS FPC diffractive data (continued)

$x_{I\!P}$	β	Q^2 (GeV^2)	$x_{I\!P}F_2^{D(3)}$	Δ_{stat}	Δ_{syst}
0.00993	0.1429	6.0	0.0243	± 0.0020	$^{+0.0019}_{-0.0021}$
0.00581	0.1429	6.0	0.0254	± 0.0018	$^{+0.0009}_{-0.0025}$
0.00317	0.1429	6.0	0.0249	± 0.0016	$^{+0.0012}_{-0.0006}$
0.00187	0.1429	6.0	0.0323	± 0.0022	$^{+0.0021}_{-0.0021}$
0.00130	0.1429	6.0	0.0319	± 0.0020	$^{+0.0015}_{-0.0020}$
0.00087	0.1429	6.0	0.0370	± 0.0023	$^{+0.0018}_{-0.0013}$
0.01756	0.0472	6.0	0.0168	± 0.0037	$^{+0.0041}_{-0.0022}$
0.00960	0.0472	6.0	0.0233	± 0.0022	$^{+0.0013}_{-0.0028}$
0.00564	0.0472	6.0	0.0211	± 0.0019	$^{+0.0018}_{-0.0015}$
0.00392	0.0472	6.0	0.0249	± 0.0019	$^{+0.0011}_{-0.0015}$
0.00262	0.0472	6.0	0.0316	± 0.0022	$^{+0.0010}_{-0.0012}$
0.01804	0.0148	6.0	0.0225	± 0.0058	$^{+0.0035}_{-0.0029}$
0.01253	0.0148	6.0	0.0236	± 0.0036	$^{+0.0017}_{-0.0037}$
0.00839	0.0148	6.0	0.0260	± 0.0027	$^{+0.0024}_{-0.0027}$
0.01872	0.0066	6.0	0.0235	± 0.0068	$^{+0.0044}_{-0.0034}$
0.00464	0.8475	8.0	0.0315	± 0.0021	$^{+0.0037}_{-0.0029}$
0.00223	0.8475	8.0	0.0347	± 0.0023	$^{+0.0047}_{-0.0042}$
0.00131	0.8475	8.0	0.0366	± 0.0024	$^{+0.0056}_{-0.0041}$
0.00071	0.8475	8.0	0.0423	± 0.0027	$^{+0.0049}_{-0.0033}$
0.00042	0.8475	8.0	0.0448	± 0.0033	$^{+0.0038}_{-0.0034}$
0.00029	0.8475	8.0	0.0507	± 0.0035	$^{+0.0040}_{-0.0065}$
0.00020	0.8475	8.0	0.0421	± 0.0037	$^{+0.0075}_{-0.0045}$
0.00836	0.4706	8.0	0.0338	± 0.0019	$^{+0.0013}_{-0.0008}$
0.00402	0.4706	8.0	0.0380	± 0.0022	$^{+0.0025}_{-0.0045}$
0.00235	0.4706	8.0	0.0438	± 0.0024	$^{+0.0051}_{-0.0026}$
0.00129	0.4706	8.0	0.0431	± 0.0023	$^{+0.0012}_{-0.0017}$
0.00076	0.4706	8.0	0.0516	± 0.0031	$^{+0.0036}_{-0.0035}$
0.00052	0.4706	8.0	0.0487	± 0.0029	$^{+0.0039}_{-0.0014}$
0.00035	0.4706	8.0	0.0556	± 0.0034	$^{+0.0039}_{-0.0033}$
0.02164	0.1818	8.0	0.0210	± 0.0035	$^{+0.0020}_{-0.0015}$
0.01039	0.1818	8.0	0.0233	± 0.0017	$^{+0.0018}_{-0.0016}$
0.00608	0.1818	8.0	0.0269	± 0.0016	$^{+0.0032}_{-0.0020}$
0.00332	0.1818	8.0	0.0298	± 0.0016	$^{+0.0006}_{-0.0013}$
0.00195	0.1818	8.0	0.0290	± 0.0018	$^{+0.0014}_{-0.0016}$
0.00136	0.1818	8.0	0.0351	± 0.0020	$^{+0.0023}_{-0.0019}$
0.00091	0.1818	8.0	0.0385	± 0.0022	$^{+0.0012}_{-0.0021}$
0.01783	0.0620	8.0	0.0209	± 0.0039	$^{+0.0022}_{-0.0039}$

Table 2: ZEUS FPC diffractive data (continued)

$x_{I\!P}$	β	$Q^2\,(\mathrm{GeV}^2)$	$x_{I\!P}F_2^{D(3)}$	Δ_{stat}	Δ_{syst}
0.00975	0.0620	8.0	0.0261	± 0.0022	$^{+0.0017}_{-0.0011}$
0.00573	0.0620	8.0	0.0253	± 0.0019	$^{+0.0014}_{-0.0008}$
0.00398	0.0620	8.0	0.0271	± 0.0019	$^{+0.0008}_{-0.0015}$
0.00267	0.0620	8.0	0.0308	± 0.0020	$^{+0.0022}_{-0.0007}$
0.01813	0.0196	8.0	0.0227	± 0.0056	$^{+0.0026}_{-0.0025}$
0.01259	0.0196	8.0	0.0302	± 0.0038	$^{+0.0018}_{-0.0036}$
0.00843	0.0196	8.0	0.0302	± 0.0030	$^{+0.0024}_{-0.0037}$
0.01876	0.0088	8.0	0.0256	± 0.0075	$^{+0.0054}_{-0.0023}$
0.00757	0.9067	14.0	0.0262	± 0.0017	$^{+0.0038}_{-0.0025}$
0.00364	0.9067	14.0	0.0257	± 0.0018	$^{+0.0033}_{-0.0034}$
0.00213	0.9067	14.0	0.0332	± 0.0021	$^{+0.0046}_{-0.0054}$
0.00117	0.9067	14.0	0.0328	± 0.0021	$^{+0.0033}_{-0.0026}$
0.00069	0.9067	14.0	0.0354	± 0.0027	$^{+0.0031}_{-0.0034}$
0.00048	0.9067	14.0	0.0266	± 0.0023	$^{+0.0030}_{-0.0025}$
0.00032	0.9067	14.0	0.0434	± 0.0037	$^{+0.0049}_{-0.0042}$
0.01128	0.6087	14.0	0.0309	± 0.0016	$^{+0.0014}_{-0.0019}$
0.00543	0.6087	14.0	0.0344	± 0.0018	$^{+0.0036}_{-0.0023}$
0.00318	0.6087	14.0	0.0406	± 0.0019	$^{+0.0064}_{-0.0043}$
0.00174	0.6087	14.0	0.0444	± 0.0021	$^{+0.0011}_{-0.0027}$
0.00102	0.6087	14.0	0.0450	± 0.0025	$^{+0.0035}_{-0.0018}$
0.00071	0.6087	14.0	0.0519	± 0.0028	$^{+0.0054}_{-0.0045}$
0.00048	0.6087	14.0	0.0569	± 0.0034	$^{+0.0048}_{-0.0037}$
0.02452	0.2800	14.0	0.0199	± 0.0039	$^{+0.0017}_{-0.0016}$
0.01180	0.2800	14.0	0.0248	± 0.0017	$^{+0.0026}_{-0.0026}$
0.00691	0.2800	14.0	0.0304	± 0.0014	$^{+0.0037}_{-0.0029}$
0.00378	0.2800	14.0	0.0317	± 0.0014	$^{+0.0005}_{-0.0028}$
0.00222	0.2800	14.0	0.0357	± 0.0018	$^{+0.0015}_{-0.0010}$
0.00154	0.2800	14.0	0.0405	± 0.0019	$^{+0.0010}_{-0.0013}$
0.00103	0.2800	14.0	0.0403	± 0.0021	$^{+0.0024}_{-0.0017}$
0.01865	0.1037	14.0	0.0239	± 0.0040	$^{+0.0044}_{-0.0039}$
0.01020	0.1037	14.0	0.0258	± 0.0020	$^{+0.0013}_{-0.0021}$
0.00600	0.1037	14.0	0.0277	± 0.0018	$^{+0.0009}_{-0.0014}$
0.00416	0.1037	14.0	0.0303	± 0.0017	$^{+0.0016}_{-0.0013}$
0.00279	0.1037	14.0	0.0350	± 0.0020	$^{+0.0011}_{-0.0009}$
0.01839	0.0338	14.0	0.0231	± 0.0059	$^{+0.0033}_{-0.0028}$
0.01277	0.0338	14.0	0.0278	± 0.0038	$^{+0.0019}_{-0.0022}$
0.00855	0.0338	14.0	0.0322	± 0.0028	$^{+0.0019}_{-0.0019}$

Table 2: ZEUS FPC diffractive data (continued)

$x_{I\!P}$	β	Q^2 (GeV^2)	$x_{I\!P}F_2^{D(3)}$	Δ_{stat}	Δ_{syst}
0.01888	0.0153	14.0	0.0325	± 0.0080	$^{+0.0039}_{-0.0032}$
0.01386	0.9494	27.0	0.0192	± 0.0028	$^{+0.0025}_{-0.0034}$
0.00669	0.9494	27.0	0.0168	± 0.0029	$^{+0.0031}_{-0.0017}$
0.00392	0.9494	27.0	0.0270	± 0.0036	$^{+0.0039}_{-0.0044}$
0.00215	0.9494	27.0	0.0160	± 0.0029	$^{+0.0033}_{-0.0024}$
0.00126	0.9494	27.0	0.0372	± 0.0060	$^{+0.0016}_{-0.0108}$
0.00088	0.9494	27.0	0.0268	± 0.0049	$^{+0.0041}_{-0.0046}$
0.00059	0.9494	27.0	0.0290	± 0.0054	$^{+0.0058}_{-0.0028}$
0.01754	0.7500	27.0	0.0165	± 0.0019	$^{+0.0023}_{-0.0018}$
0.00847	0.7500	27.0	0.0256	± 0.0027	$^{+0.0062}_{-0.0032}$
0.00496	0.7500	27.0	0.0310	± 0.0028	$^{+0.0048}_{-0.0055}$
0.00272	0.7500	27.0	0.0363	± 0.0031	$^{+0.0034}_{-0.0031}$
0.00160	0.7500	27.0	0.0433	± 0.0044	$^{+0.0035}_{-0.0051}$
0.00111	0.7500	27.0	0.0444	± 0.0046	$^{+0.0065}_{-0.0030}$
0.00074	0.7500	27.0	0.0522	± 0.0049	$^{+0.0055}_{-0.0057}$
0.01482	0.4286	27.0	0.0257	± 0.0026	$^{+0.0018}_{-0.0027}$
0.00869	0.4286	27.0	0.0327	± 0.0023	$^{+0.0036}_{-0.0042}$
0.00475	0.4286	27.0	0.0380	± 0.0025	$^{+0.0020}_{-0.0042}$
0.00280	0.4286	27.0	0.0392	± 0.0030	$^{+0.0011}_{-0.0013}$
0.00194	0.4286	27.0	0.0475	± 0.0036	$^{+0.0002}_{-0.0028}$
0.00130	0.4286	27.0	0.0553	± 0.0037	$^{+0.0016}_{-0.0034}$
0.02041	0.1824	27.0	0.0201	± 0.0048	$^{+0.0052}_{-0.0027}$
0.01117	0.1824	27.0	0.0218	± 0.0028	$^{+0.0031}_{-0.0013}$
0.00657	0.1824	27.0	0.0252	± 0.0025	$^{+0.0016}_{-0.0015}$
0.00456	0.1824	27.0	0.0283	± 0.0025	$^{+0.0027}_{-0.0017}$
0.00306	0.1824	27.0	0.0389	± 0.0028	$^{+0.0010}_{-0.0030}$
0.01896	0.0632	27.0	0.0211	± 0.0067	$^{+0.0026}_{-0.0046}$
0.01317	0.0632	27.0	0.0274	± 0.0046	$^{+0.0025}_{-0.0028}$
0.00882	0.0632	27.0	0.0296	± 0.0035	$^{+0.0028}_{-0.0020}$
0.01914	0.0291	27.0	0.0249	± 0.0082	$^{+0.0037}_{-0.0041}$
0.02713	0.9745	55.0	0.0128	± 0.0045	$^{+0.0039}_{-0.0047}$
0.01319	0.9745	55.0	0.0167	± 0.0066	$^{+0.0026}_{-0.0027}$
0.00775	0.9745	55.0	0.0072	± 0.0034	$^{+0.0059}_{-0.0015}$
0.00425	0.9745	55.0	0.0146	± 0.0045	$^{+0.0015}_{-0.0026}$
0.00174	0.9745	55.0	0.0139	± 0.0036	$^{+0.0035}_{-0.0071}$
0.01495	0.8594	55.0	0.0146	± 0.0036	$^{+0.0027}_{-0.0007}$
0.00879	0.8594	55.0	0.0222	± 0.0041	$^{+0.0018}_{-0.0024}$

Table 2: ZEUS FPC diffractive data (continued)

$x_{I\!P}$	β	$Q^2\,(\mathrm{GeV}^2)$	$x_{I\!P}F_2^{D(3)}$	Δ_{stat}	Δ_{syst}
0.00482	0.8594	55.0	0.0229	± 0.0043	$^{+0.0048}_{-0.0022}$
0.00284	0.8594	55.0	0.0245	± 0.0058	$^{+0.0072}_{-0.0053}$
0.00197	0.8594	55.0	0.0335	± 0.0061	$^{+0.0027}_{-0.0081}$
0.00132	0.8594	55.0	0.0386	± 0.0072	$^{+0.0076}_{-0.0053}$
0.02126	0.6044	55.0	0.0171	± 0.0036	$^{+0.0025}_{-0.0021}$
0.01250	0.6044	55.0	0.0242	± 0.0031	$^{+0.0065}_{-0.0035}$
0.00685	0.6044	55.0	0.0329	± 0.0033	$^{+0.0016}_{-0.0041}$
0.00404	0.6044	55.0	0.0288	± 0.0040	$^{+0.0067}_{-0.0030}$
0.00280	0.6044	55.0	0.0492	± 0.0052	$^{+0.0010}_{-0.0055}$
0.00188	0.6044	55.0	0.0429	± 0.0049	$^{+0.0027}_{-0.0036}$
0.01325	0.3125	55.0	0.0295	± 0.0037	$^{+0.0018}_{-0.0029}$
0.00780	0.3125	55.0	0.0303	± 0.0037	$^{+0.0034}_{-0.0025}$
0.00542	0.3125	55.0	0.0381	± 0.0038	$^{+0.0032}_{-0.0007}$
0.00363	0.3125	55.0	0.0442	± 0.0045	$^{+0.0017}_{-0.0026}$
0.02017	0.1209	55.0	0.0236	± 0.0075	$^{+0.0049}_{-0.0060}$
0.01402	0.1209	55.0	0.0223	± 0.0051	$^{+0.0028}_{-0.0030}$
0.00939	0.1209	55.0	0.0286	± 0.0047	$^{+0.0062}_{-0.0024}$

Table 3: ZEUS LPS diffractive data

$x_{I\!P}$	β	Q^2 (GeV^2)	$x_{I\!P}F_2^{D(3)}$	Δ_{stat}
0.00680	0.007	2.4	0.01168	±0.00414
0.01900	0.007	2.4	0.01455	±0.00229
0.04000	0.007	2.4	0.01662	±0.00319
0.06000	0.007	2.4	0.02122	±0.00235
0.00280	0.030	2.4	0.01407	±0.00377
0.00680	0.030	2.4	0.01395	±0.00349
0.01900	0.030	2.4	0.01230	±0.00247
0.04000	0.030	2.4	0.01505	±0.00233
0.06000	0.030	2.4	0.02180	±0.00314
0.00050	0.130	2.4	0.01633	±0.00331
0.00120	0.130	2.4	0.01836	±0.00346
0.00280	0.130	2.4	0.01312	±0.00280
0.00680	0.130	2.4	0.01642	±0.00348
0.01900	0.130	2.4	0.01728	±0.00333
0.00050	0.480	2.4	0.03312	±0.00561
0.00120	0.480	2.4	0.02708	±0.00535
0.00280	0.480	2.4	0.01807	±0.00398
0.01900	0.007	3.7	0.01337	±0.00225
0.04000	0.007	3.7	0.01826	±0.00269
0.06000	0.007	3.7	0.02818	±0.00389
0.00280	0.030	3.7	0.02056	±0.00577
0.00680	0.030	3.7	0.01913	±0.00455
0.01900	0.030	3.7	0.01016	±0.00315
0.04000	0.030	3.7	0.01338	±0.00224
0.06000	0.030	3.7	0.02109	±0.00224
0.00050	0.130	3.7	0.02429	±0.00596
0.00120	0.130	3.7	0.01944	±0.00368
0.00280	0.130	3.7	0.01423	±0.00274
0.00680	0.130	3.7	0.00873	±0.00189
0.01900	0.130	3.7	0.01059	±0.00163
0.04000	0.130	3.7	0.00887	±0.00186
0.00050	0.480	3.7	0.04234	±0.00564
0.00120	0.480	3.7	0.03555	±0.00585
0.00280	0.480	3.7	0.02774	±0.00618
0.00680	0.480	3.7	0.02339	±0.00456
0.01900	0.007	6.9	0.01817	±0.00314
0.04000	0.007	6.9	0.02496	±0.00300

Table 3: ZEUS LPS diffractive data (continued)

$x_{I\!P}$	β	Q^2 (GeV^2)	$x_{I\!P} F_2^{D(3)}$	Δ_{stat}
0.06000	0.007	6.9	0.02744	±0.00240
0.00680	0.030	6.9	0.02057	±0.00383
0.01900	0.030	6.9	0.01376	±0.00169
0.04000	0.030	6.9	0.01393	±0.00311
0.06000	0.030	6.9	0.02813	±0.00317
0.00120	0.130	6.9	0.02369	±0.00443
0.00280	0.130	6.9	0.01957	±0.00318
0.00680	0.130	6.9	0.01140	±0.00200
0.01900	0.130	6.9	0.01358	±0.00183
0.04000	0.130	6.9	0.01467	±0.00260
0.06000	0.130	6.9	0.01902	±0.00333
0.00050	0.480	6.9	0.04360	±0.00531
0.00120	0.480	6.9	0.03326	±0.00431
0.00280	0.480	6.9	0.02745	±0.00421
0.00680	0.480	6.9	0.02602	±0.00409
0.01900	0.480	6.9	0.01561	±0.00281
0.04000	0.007	13.5	0.04063	±0.00730
0.06000	0.007	13.5	0.04203	±0.00461
0.01900	0.030	13.5	0.02074	±0.00388
0.04000	0.030	13.5	0.02641	±0.00374
0.06000	0.030	13.5	0.03027	±0.00319
0.00280	0.130	13.5	0.02103	±0.00464
0.00680	0.130	13.5	0.01649	±0.00282
0.01900	0.130	13.5	0.01565	±0.00208
0.04000	0.130	13.5	0.01753	±0.00266
0.06000	0.130	13.5	0.02095	±0.00267
0.00050	0.480	13.5	0.04832	±0.01076
0.00120	0.480	13.5	0.03259	±0.00462
0.00280	0.480	13.5	0.02617	±0.00400
0.00680	0.480	13.5	0.02018	±0.00313
0.01900	0.480	13.5	0.02358	±0.00408
0.04000	0.480	13.5	0.01399	±0.00296
0.04000	0.030	39.0	0.03789	±0.00662
0.06000	0.030	39.0	0.03938	±0.00448
0.00680	0.130	39.0	0.03030	±0.00698
0.01900	0.130	39.0	0.02225	±0.00329
0.04000	0.130	39.0	0.02027	±0.00332

Table 3: ZEUS LPS diffractive data (continued)

$x_{I\!P}$	β	Q^2 (GeV^2)	$x_{I\!P}F_2^{D(3)}$	Δ_{stat}
0.06000	0.130	39.0	0.02893	$\pm$0.00332
0.00280	0.480	39.0	0.02872	$\pm$0.00556
0.00680	0.480	39.0	0.02119	$\pm$0.00414
0.01900	0.480	39.0	0.01757	$\pm$0.00293
0.04000	0.480	39.0	0.02004	$\pm$0.00416
0.06000	0.480	39.0	0.01900	$\pm$0.00328

Table 4: H1 diffractive data

$x_{I\!P}$	β	Q^2 (GeV^2)	$x_{I\!P} F_2^{D(3)}$	Δ_{stat}
0.02	0.01	6.5	0.023	$\pm$0.003
0.005	0.04	6.5	0.021	$\pm$0.003
0.008	0.04	6.5	0.022	$\pm$0.004
0.013	0.04	6.5	0.023	$\pm$0.004
0.02	0.04	6.5	0.020	$\pm$0.003
0.002	0.1	6.5	0.024	$\pm$0.004
0.0032	0.1	6.5	0.018	$\pm$0.003
0.005	0.1	6.5	0.015	$\pm$0.004
0.008	0.1	6.5	0.012	$\pm$0.002
0.013	0.1	6.5	0.018	$\pm$0.003
0.001	0.2	6.5	0.029	$\pm$0.005
0.0016	0.2	6.5	0.024	$\pm$0.004
0.0025	0.2	6.5	0.016	$\pm$0.003
0.004	0.2	6.5	0.026	$\pm$0.005
0.0064	0.2	6.5	0.016	$\pm$0.003
0.0005	0.4	6.5	0.055	$\pm$0.008
0.0008	0.4	6.5	0.035	$\pm$0.006
0.0013	0.4	6.5	0.038	$\pm$0.009
0.002	0.4	6.5	0.033	$\pm$0.005
0.0032	0.4	6.5	0.027	$\pm$0.006
0.00031	0.65	6.5	0.048	$\pm$0.008
0.00049	0.65	6.5	0.037	$\pm$0.011
0.00078	0.65	6.5	0.049	$\pm$0.014
0.0012	0.65	6.5	0.049	$\pm$0.010
0.002	0.65	6.5	0.028	$\pm$0.005
0.00022	0.9	6.5	0.055	$\pm$0.015
0.00036	0.9	6.5	0.050	$\pm$0.009
0.00056	0.9	6.5	0.028	$\pm$0.007
0.00089	0.9	6.5	0.047	$\pm$0.010
0.0014	0.9	6.5	0.042	$\pm$0.015
0.02	0.01	8.5	0.030	$\pm$0.003
0.005	0.04	8.5	0.018	$\pm$0.002
0.008	0.04	8.5	0.023	$\pm$0.002
0.013	0.04	8.5	0.022	$\pm$0.002
0.02	0.04	8.5	0.021	$\pm$0.003
0.002	0.1	8.5	0.022	$\pm$0.004
0.0032	0.1	8.5	0.021	$\pm$0.003

Table 4: H1 diffractive data (continued)

$x_{I\!P}$	β	Q^2 (GeV^2)	$x_{I\!P}F_2^{D(3)}$	Δ_{stat}
0.005	0.1	8.5	0.019	$\pm$0.003
0.008	0.1	8.5	0.015	$\pm$0.002
0.013	0.1	8.5	0.018	$\pm$0.002
0.02	0.1	8.5	0.023	$\pm$0.004
0.001	0.2	8.5	0.025	$\pm$0.003
0.0016	0.2	8.5	0.023	$\pm$0.003
0.0025	0.2	8.5	0.021	$\pm$0.003
0.004	0.2	8.5	0.022	$\pm$0.005
0.0064	0.2	8.5	0.017	$\pm$0.002
0.01	0.2	8.5	0.016	$\pm$0.002
0.0005	0.4	8.5	0.051	$\pm$0.006
0.0008	0.4	8.5	0.044	$\pm$0.005
0.0013	0.4	8.5	0.039	$\pm$0.005
0.002	0.4	8.5	0.038	$\pm$0.005
0.0032	0.4	8.5	0.026	$\pm$0.004
0.005	0.4	8.5	0.026	$\pm$0.004
0.00031	0.65	8.5	0.053	$\pm$0.008
0.00049	0.65	8.5	0.050	$\pm$0.006
0.00078	0.65	8.5	0.039	$\pm$0.005
0.0012	0.65	8.5	0.045	$\pm$0.006
0.002	0.65	8.5	0.037	$\pm$0.005
0.0031	0.65	8.5	0.037	$\pm$0.007
0.00036	0.9	8.5	0.037	$\pm$0.007
0.00056	0.9	8.5	0.045	$\pm$0.008
0.00089	0.9	8.5	0.048	$\pm$0.015
0.0014	0.9	8.5	0.032	$\pm$0.006
0.0022	0.9	8.5	0.027	$\pm$0.006
0.02	0.01	12	0.035	$\pm$0.005
0.005	0.04	12	0.032	$\pm$0.005
0.008	0.04	12	0.027	$\pm$0.003
0.013	0.04	12	0.029	$\pm$0.003
0.02	0.04	12	0.033	$\pm$0.004
0.002	0.1	12	0.022	$\pm$0.004
0.0032	0.1	12	0.021	$\pm$0.003
0.005	0.1	12	0.019	$\pm$0.003
0.008	0.1	12	0.026	$\pm$0.003
0.013	0.1	12	0.027	$\pm$0.004

Table 4: H1 diffractive data (continued)

$x_{I\!P}$	β	Q^2 (GeV^2)	$x_{I\!P} F_2^{D(3)}$	Δ_{stat}
0.02	0.1	12	0.025	$\pm$0.007
0.001	0.2	12	0.039	$\pm$0.007
0.0016	0.2	12	0.029	$\pm$0.004
0.0025	0.2	12	0.030	$\pm$0.004
0.004	0.2	12	0.020	$\pm$0.003
0.0064	0.2	12	0.017	$\pm$0.002
0.01	0.2	12	0.021	$\pm$0.003
0.0005	0.4	12	0.051	$\pm$0.011
0.0008	0.4	12	0.047	$\pm$0.006
0.0013	0.4	12	0.032	$\pm$0.005
0.002	0.4	12	0.029	$\pm$0.004
0.0032	0.4	12	0.025	$\pm$0.004
0.005	0.4	12	0.023	$\pm$0.004
0.008	0.4	12	0.021	$\pm$0.004
0.00031	0.65	12	0.083	$\pm$0.018
0.00049	0.65	12	0.042	$\pm$0.006
0.00078	0.65	12	0.050	$\pm$0.007
0.0012	0.65	12	0.048	$\pm$0.006
0.002	0.65	12	0.036	$\pm$0.005
0.0031	0.65	12	0.027	$\pm$0.005
0.0049	0.65	12	0.042	$\pm$0.008
0.00036	0.9	12	0.044	$\pm$0.012
0.00056	0.9	12	0.026	$\pm$0.006
0.00089	0.9	12	0.030	$\pm$0.006
0.0014	0.9	12	0.037	$\pm$0.007
0.0022	0.9	12	0.031	$\pm$0.006
0.0036	0.9	12	0.038	$\pm$0.012
0.02	0.01	15	0.058	$\pm$0.012
0.005	0.04	15	0.033	$\pm$0.006
0.008	0.04	15	0.028	$\pm$0.002
0.013	0.04	15	0.026	$\pm$0.002
0.02	0.04	15	0.028	$\pm$0.002
0.002	0.1	15	0.036	$\pm$0.009
0.0032	0.1	15	0.028	$\pm$0.002
0.005	0.1	15	0.024	$\pm$0.002
0.008	0.1	15	0.020	$\pm$0.002
0.013	0.1	15	0.020	$\pm$0.001

Table 4: H1 diffractive data (continued)

$x_{I\!P}$	β	Q^2 (GeV^2)	$x_{I\!P}F_2^{D(3)}$	Δ_{stat}
0.02	0.1	15	0.025	$\pm$0.002
0.001	0.2	15	0.064	$\pm$0.013
0.0016	0.2	15	0.032	$\pm$0.002
0.0025	0.2	15	0.026	$\pm$0.002
0.004	0.2	15	0.025	$\pm$0.002
0.0064	0.2	15	0.023	$\pm$0.001
0.01	0.2	15	0.020	$\pm$0.001
0.016	0.2	15	0.020	$\pm$0.001
0.0005	0.4	15	0.039	$\pm$0.010
0.0008	0.4	15	0.045	$\pm$0.004
0.0013	0.4	15	0.045	$\pm$0.003
0.002	0.4	15	0.035	$\pm$0.003
0.0032	0.4	15	0.028	$\pm$0.002
0.005	0.4	15	0.027	$\pm$0.002
0.008	0.4	15	0.024	$\pm$0.002
0.00049	0.65	15	0.056	$\pm$0.005
0.00078	0.65	15	0.045	$\pm$0.003
0.0012	0.65	15	0.043	$\pm$0.003
0.002	0.65	15	0.041	$\pm$0.003
0.0031	0.65	15	0.032	$\pm$0.002
0.0049	0.65	15	0.031	$\pm$0.002
0.00036	0.9	15	0.035	$\pm$0.008
0.00056	0.9	15	0.033	$\pm$0.005
0.00089	0.9	15	0.026	$\pm$0.003
0.0014	0.9	15	0.030	$\pm$0.003
0.0022	0.9	15	0.037	$\pm$0.004
0.0036	0.9	15	0.025	$\pm$0.003
0.008	0.04	20	0.033	$\pm$0.003
0.013	0.04	20	0.030	$\pm$0.002
0.02	0.04	20	0.031	$\pm$0.002
0.0032	0.1	20	0.033	$\pm$0.004
0.005	0.1	20	0.026	$\pm$0.002
0.008	0.1	20	0.025	$\pm$0.002
0.013	0.1	20	0.023	$\pm$0.002
0.02	0.1	20	0.023	$\pm$0.002
0.0016	0.2	20	0.035	$\pm$0.004
0.0025	0.2	20	0.030	$\pm$0.002

Table 4: H1 diffractive data (continued)

$x_{I\!P}$	β	Q^2 (GeV^2)	$x_{I\!P} F_2^{D(3)}$	Δ_{stat}
0.004	0.2	20	0.030	$\pm$0.002
0.0064	0.2	20	0.027	$\pm$0.002
0.01	0.2	20	0.024	$\pm$0.002
0.016	0.2	20	0.021	$\pm$0.002
0.025	0.2	20	0.022	$\pm$0.002
0.0008	0.4	20	0.036	$\pm$0.005
0.0013	0.4	20	0.039	$\pm$0.003
0.002	0.4	20	0.036	$\pm$0.004
0.0032	0.4	20	0.027	$\pm$0.002
0.005	0.4	20	0.020	$\pm$0.005
0.008	0.4	20	0.025	$\pm$0.002
0.013	0.4	20	0.024	$\pm$0.003
0.00049	0.65	20	0.052	$\pm$0.007
0.00078	0.65	20	0.051	$\pm$0.004
0.0012	0.65	20	0.046	$\pm$0.003
0.002	0.65	20	0.040	$\pm$0.003
0.0031	0.65	20	0.040	$\pm$0.003
0.0049	0.65	20	0.033	$\pm$0.003
0.0078	0.65	20	0.024	$\pm$0.003
0.00036	0.9	20	0.025	$\pm$0.008
0.00056	0.9	20	0.034	$\pm$0.006
0.00089	0.9	20	0.030	$\pm$0.004
0.0014	0.9	20	0.037	$\pm$0.004
0.0022	0.9	20	0.031	$\pm$0.004
0.0036	0.9	20	0.014	$\pm$0.009
0.0056	0.9	20	0.027	$\pm$0.005
0.008	0.04	25	0.023	$\pm$0.006
0.013	0.04	25	0.033	$\pm$0.003
0.02	0.04	25	0.037	$\pm$0.003
0.005	0.1	25	0.026	$\pm$0.003
0.008	0.1	25	0.029	$\pm$0.002
0.013	0.1	25	0.025	$\pm$0.002
0.02	0.1	25	0.023	$\pm$0.002
0.0016	0.2	25	0.038	$\pm$0.011
0.0025	0.2	25	0.038	$\pm$0.003
0.004	0.2	25	0.028	$\pm$0.003
0.0064	0.2	25	0.026	$\pm$0.002

Table 4: H1 diffractive data (continued)

$x_{I\!P}$	β	Q^2 (GeV^2)	$x_{I\!P}F_2^{D(3)}$	Δ_{stat}
0.01	0.2	25	0.025	$\pm$0.002
0.016	0.2	25	0.023	$\pm$0.002
0.025	0.2	25	0.023	$\pm$0.002
0.0008	0.4	25	0.046	$\pm$0.015
0.0013	0.4	25	0.056	$\pm$0.007
0.002	0.4	25	0.046	$\pm$0.004
0.0032	0.4	25	0.034	$\pm$0.003
0.005	0.4	25	0.028	$\pm$0.002
0.008	0.4	25	0.027	$\pm$0.002
0.013	0.4	25	0.021	$\pm$0.002
0.00049	0.65	25	0.058	$\pm$0.024
0.00078	0.65	25	0.051	$\pm$0.005
0.0012	0.65	25	0.051	$\pm$0.004
0.002	0.65	25	0.042	$\pm$0.003
0.0031	0.65	25	0.037	$\pm$0.003
0.0049	0.65	25	0.032	$\pm$0.003
0.0078	0.65	25	0.030	$\pm$0.003
0.00056	0.9	25	0.031	$\pm$0.008
0.00089	0.9	25	0.025	$\pm$0.004
0.0014	0.9	25	0.032	$\pm$0.005
0.0022	0.9	25	0.023	$\pm$0.003
0.0036	0.9	25	0.019	$\pm$0.003
0.0056	0.9	25	0.022	$\pm$0.003
0.013	0.04	35	0.028	$\pm$0.005
0.02	0.04	35	0.039	$\pm$0.003
0.005	0.1	35	0.042	$\pm$0.009
0.008	0.1	35	0.027	$\pm$0.003
0.013	0.1	35	0.027	$\pm$0.003
0.02	0.1	35	0.029	$\pm$0.003
0.0025	0.2	35	0.049	$\pm$0.009
0.004	0.2	35	0.038	$\pm$0.003
0.0064	0.2	35	0.026	$\pm$0.002
0.01	0.2	35	0.027	$\pm$0.002
0.016	0.2	35	0.025	$\pm$0.002
0.025	0.2	35	0.027	$\pm$0.003
0.0013	0.4	35	0.047	$\pm$0.009
0.002	0.4	35	0.048	$\pm$0.005

Table 4: H1 diffractive data (continued)

$x_{I\!P}$	β	Q^2 (GeV^2)	$x_{I\!P} F_2^{D(3)}$	Δ_{stat}
0.0032	0.4	35	0.035	$\pm$0.004
0.005	0.4	35	0.029	$\pm$0.003
0.008	0.4	35	0.023	$\pm$0.002
0.013	0.4	35	0.024	$\pm$0.002
0.02	0.4	35	0.027	$\pm$0.003
0.00078	0.65	35	0.079	$\pm$0.014
0.0012	0.65	35	0.041	$\pm$0.004
0.002	0.65	35	0.042	$\pm$0.004
0.0031	0.65	35	0.037	$\pm$0.004
0.0049	0.65	35	0.031	$\pm$0.003
0.0078	0.65	35	0.033	$\pm$0.005
0.012	0.65	35	0.037	$\pm$0.005
0.00056	0.9	35	0.010	$\pm$0.007
0.00089	0.9	35	0.023	$\pm$0.006
0.0014	0.9	35	0.026	$\pm$0.005
0.0022	0.9	35	0.021	$\pm$0.003
0.0036	0.9	35	0.027	$\pm$0.004
0.0056	0.9	35	0.016	$\pm$0.003
0.0089	0.9	35	0.020	$\pm$0.004
0.02	0.04	45	0.045	$\pm$0.007
0.008	0.1	45	0.035	$\pm$0.006
0.013	0.1	45	0.033	$\pm$0.004
0.02	0.1	45	0.030	$\pm$0.004
0.004	0.2	45	0.041	$\pm$0.006
0.0064	0.2	45	0.033	$\pm$0.003
0.01	0.2	45	0.025	$\pm$0.003
0.016	0.2	45	0.016	$\pm$0.003
0.025	0.2	45	0.025	$\pm$0.003
0.002	0.4	45	0.036	$\pm$0.007
0.0032	0.4	45	0.034	$\pm$0.004
0.005	0.4	45	0.030	$\pm$0.004
0.008	0.4	45	0.032	$\pm$0.004
0.013	0.4	45	0.032	$\pm$0.004
0.02	0.4	45	0.021	$\pm$0.003
0.0012	0.65	45	0.048	$\pm$0.009
0.002	0.65	45	0.042	$\pm$0.006
0.0031	0.65	45	0.037	$\pm$0.004

Table 4: H1 diffractive data (continued)

$x_{I\!P}$	β	Q^2 (GeV^2)	$x_{I\!P}F_2^{D(3)}$	Δ_{stat}
0.0049	0.65	45	0.027	$\pm$0.003
0.0078	0.65	45	0.032	$\pm$0.004
0.012	0.65	45	0.023	$\pm$0.003
0.00089	0.9	45	0.010	$\pm$0.011
0.0014	0.9	45	0.030	$\pm$0.009
0.0022	0.9	45	0.026	$\pm$0.006
0.0036	0.9	45	0.026	$\pm$0.006
0.0056	0.9	45	0.032	$\pm$0.007
0.0089	0.9	45	0.016	$\pm$0.004
0.013	0.1	60	0.041	$\pm$0.007
0.02	0.1	60	0.038	$\pm$0.005
0.0064	0.2	60	0.044	$\pm$0.007
0.01	0.2	60	0.027	$\pm$0.003
0.016	0.2	60	0.024	$\pm$0.003
0.025	0.2	60	0.026	$\pm$0.003
0.0032	0.4	60	0.041	$\pm$0.008
0.005	0.4	60	0.031	$\pm$0.004
0.008	0.4	60	0.028	$\pm$0.004
0.013	0.4	60	0.029	$\pm$0.006
0.02	0.4	60	0.026	$\pm$0.006
0.032	0.4	60	0.025	$\pm$0.004
0.002	0.65	60	0.037	$\pm$0.008
0.0031	0.65	60	0.036	$\pm$0.005
0.0049	0.65	60	0.032	$\pm$0.004
0.0078	0.65	60	0.028	$\pm$0.004
0.012	0.65	60	0.021	$\pm$0.003
0.02	0.65	60	0.022	$\pm$0.004
0.0014	0.9	60	0.015	$\pm$0.015
0.0022	0.9	60	0.024	$\pm$0.007
0.0036	0.9	60	0.025	$\pm$0.006
0.0056	0.9	60	0.026	$\pm$0.006
0.0089	0.9	60	0.026	$\pm$0.005
0.014	0.9	60	0.023	$\pm$0.006
0.016	0.2	90	0.037	$\pm$0.007
0.025	0.2	90	0.041	$\pm$0.006
0.008	0.4	90	0.030	$\pm$0.007
0.013	0.4	90	0.028	$\pm$0.005

Table 4: H1 diffractive data (continued)

$x_{I\!P}$	β	Q^2 (GeV^2)	$x_{I\!P} F_2^{D(3)}$	Δ_{stat}
0.02	0.4	90	0.021	$\pm$0.004
0.032	0.4	90	0.025	$\pm$0.005
0.0049	0.65	90	0.032	$\pm$0.008
0.0078	0.65	90	0.024	$\pm$0.005
0.012	0.65	90	0.029	$\pm$0.005
0.02	0.65	90	0.018	$\pm$0.003
0.0036	0.9	90	0.029	$\pm$0.011
0.0056	0.9	90	0.015	$\pm$0.006
0.0089	0.9	90	0.016	$\pm$0.006
0.014	0.9	90	0.018	$\pm$0.006
0.022	0.9	90	0.012	$\pm$0.004
0.032	0.4	120	0.011	$\pm$0.007
0.02	0.65	120	0.019	$\pm$0.008
0.031	0.65	120	0.025	$\pm$0.009
0.049	0.65	120	0.017	$\pm$0.011
0.022	0.9	120	0.004	$\pm$0.004